A transient mechanical crosstalk between Adherens Junctions and Focal Adhesions sustains cell proliferation in premalignant breast epithelial cells

Lídia Faria*(1, 2, 3), Carine M Gonçalves* (1, 2), Inês Fidalgo (1, 2, 4), Carla S. Lopes (1, 5); Vanessa Rodrigues (1,2); Maria M. Azevedo (1, 5); Paula Sampaio (1, 5); Sandra Tavares (1, 2); Vaibhav Mahajan (6); Anna Taubenberger (6); and Florence Janody (1, 2)±

(1) Instituto de Investigação e Inovação em Saúde (i3S), Universidade do Porto, Rua Alfredo Allen, 208, 4200-135 Porto, Portugal.
(2) Instituto de Patologia e Imunologia Molecular da Universidade do Porto (Ipatimup), Rua Júlio Amaral de Carvalho, n 45, 4200-135 Porto, Portugal.
(3) Doctoral Programme in Molecular and Cell Biology, School of Medicine & Biomedical Sciences, University of Porto (ICBAS-UP), Rua Jorge Viterbo Ferreira 228, 4050-513 Porto, Portugal.
(4) Master Programme in Oncology, School of Medicine & Biomedical Sciences, University of Porto (ICBAS-UP), Rua Jorge Viterbo Ferreira 228, 4050-513 Porto, Portugal.
(5) Instituto de Biologia Molecular e Celular (IBMC), Universidade do Porto, Rua Alfredo Allen 208, 4200-135, Porto, Portugal.
(6) Biotechnology Center, Technische Universität Dresden, Tatzberg 47/49, 01307 Dresden, Germany.

* These authors contributed equally to this work.
±corresponding author:
e-mail: fjanody@i3s.up.pt
Tel. (+351) 22 557 0730

Running Title: Force transmission between adhesion sites in cellular transformation

Abstract

The weakening of Adherens Junctions (AJs) and Focal Adhesions (FAs) adhesiveness has been proposed to enable the initiation and progression of several types of cancer. Here, we demonstrate that prior to acquiring malignant features, a transient mechanical crosstalk between AJs and FAs provides a proliferative advantage to mammary epithelial cells overactivating the Src kinase proto-oncogene. We show that AJs and FAs are transiently under high tension during the early phase of cellular transformation. Preventing the strengthening of tensile forces at FAs by knocking down PXN or inhibiting FAK activity, suppresses the cell abilities to build up tension at AJs and to grow. Conversely, disrupting the *trans* junctional homophilic interactions between cadherin extracellular domains with EGTA or preventing AJ strengthening by knocking down P-cadherin, impedes the transient increase in tensile forces at FAs, the activation of EGFR-ERK and MRTF-A-SRF signalling and cell proliferation. Moreover, knocking down E-cadherin, the sole classical cadherin in *Drosophila*, inhibits the growth of Src-overexpressing tissues *in vivo*. Thus, prior to the loss of cell-cell and cell-matrix adhesiveness, a transient mechanical crosstalk between AJs and FAs could drive tumour growth.

Introduction

Most breast cancers arise in the epithelial ducts and are referred to as ductal carcinoma. The most acknowledged model of ductal breast cancer progression states that every invasive carcinoma arises from a benign hyperplasia. These lesions are caused by excessive proliferation of the terminal duct lobular units, leading to dilated ducts, lined with one or more layers of epithelial cells (Allred et al., 2001; Allred et al., 2008; Arpino et al., 2005; Santen and Mansel, 2005). Progression of these proliferative breast lesions to invasive carcinoma has been proposed to involve a shift from an epithelial to a mesenchymal phenotype, in a process referred to as Epithelial to Mesenchymal Transition (EMT). This process is characterised by the breakdown of Adherens Junctions (AJs) and the dynamic remodelling of Focal Adhesions (FAs) (Buyuk et al., 2022).

AJs are the major cell-cell adhesion structure that senses and responds to tensile forces at the intercellular contact interface and hold epithelial cells together (Angulo-Urarte et al., 2020). AJs assemble through homotypic interactions between the extracellular domains of classical cadherins from adjacent cells in a Ca^{2+}-dependent manner. E-cadherin (Ecad) is one of the main classical cadherins, highly conserved from bilaterian metazoans to mammals and expressed in most epithelial tissues (Oda and Takeichi, 2011). Intracellularly, the Ecad cytoplasmic tail interacts with p120-catenin (p120ctn) and β-catenin (βcat). While p120ctn promotes the assembly of Ecad dimers, βcat interacts with the actin-binding protein α-catenin (αcat) and physically links AJ complexes to the actomyosin cytoskeleton in a force-dependent manner (Buckley et al., 2014; Vu et al., 2021; Yao et al., 2014). P-cadherin (Pcad), another classical cadherin, is also expressed in several epithelia, usually with Ecad (Nose and Takeichi, 1986). Alike Ecad, Pcad promotes cell-cell adhesion and Ca^{2+}-dependent cell-cell aggregation (Kudo et al., 2017; Ribeiro et al., 2013; Van Marck et al., 2005). At the cell-extracellular matrix (ECM) interface, mechanosensitive FAs assemble from nascent adhesions, which form upon the binding of a few integrin dimers to their ECM ligands and to Talin intracellularly (Tadokoro et al., 2003). The coupling of integrins to the actomyosin cytoskeleton through Talin and Paxillin recruits Vinculin, leading to the maturation of nascent adhesions into larger and more stable FAs. The mechanisms in play involve the stretching of Talin and Vinculin by tensile forces, thereby re-enforcing the connection between integrins and the actomyosin cytoskeleton and the recruitment of additional proteins, including Focal Adhesion Kinase (FAK) and Zyxin to stress fibre-bound FAs (Carisey et al., 2013; Grashoff et al., 2010). Thus, Ecad and Vinculin are *bona fide* mechanosensors (Borghi et al., 2012; Grashoff et al., 2010).

In addition to maintaining cell–cell contact and attachment to the ECM, piconewton mechanical forces transmitted at AJs and FAs expose cryptic sites within mechanosensitive proteins and modulate the binding kinetics of receptor-ligand complexes to regulate the activity of diverse mechanotransduction signalling pathways and therefore cell behaviour (Mui et al., 2016). Thus, mechanical forces associated with FAs induce the nuclear translocation of the myocardin-related transcription factor (MRTF-A), a co-factor of serum response factor (SRF), which triggers the expression of α-smooth muscle actin in fibroblasts and invasion in mammary epithelial cells (Chan et al., 2009; Gjorevski et al., 2015). Likewise, ECM-dependent FA strengthening promotes mammary epithelial cell growth through activation of extracellular signal-regulated kinase (ERK) (Provenzano et al., 2009). Increasing tension on homophilic Ecad bonds has also been shown to stimulate ERK-dependent proliferation by enabling the homodimerization of epidermal growth factor receptor (EGFR) in A-431D epithelial cells (Sullivan et al., 2022). Forces on AJs can also be transferred to FAs and *vice versa*. Integrin engagement or higher traction force from the ECM can increase tension at cell-cell contacts in multiple cell types (Martinez-Rico et al., 2010; Maruthamuthu et al., 2011). Conversely, Ecad-mediated mechanical coupling increases traction forces of murine sarcoma cancer cells and keratinocytes on fibronectin (Jasaitis et al., 2012; Mertz et al., 2013). Ecad force transmission also increases the average FA area and number and Myosin-dependent cell contractility in MCF7 cells (Muhamed et al., 2016). In turn, integrins strengthen tensile forces at AJs, thus, establishing a positive mechanotransduction feedback loop between force-activated Ecad and integrins (Sehgal et al., 2018). However, strengthening of one adhesion can also antagonize the assembly of the other (de Rooij et al., 2005; Gayrard et al., 2018). How the balance of forces between adhesion sites controls distinct outcomes during cancer progression is not fully understood.

We reported that activation of the viral non-receptor tyrosine kinase v-Src in the mammary epithelial cells MCF10A-ER-Src (ER-Src) induces transient alterations in components associated with AJs and FAs, prior to triggering EMT (Faria et al., 2023; Tavares et al., 2017). During the first 12 hours of Src activation, inducible with tamoxifen (TAM) treatment, cells transiently upregulate Ena-VASP-like (EVL). EVL accumulates at FAs where it polarises FA-associated stress fibres, triggers cell stiffening, ERK-dependent cell proliferation and their subsequent malignant progression (Tavares et al., 2017). Concomitantly, TAM-treated ER-Src cells transiently accumulate membrane-associated Pcad, which sustains cell proliferation

through a transient boost of actin-MRTF-A–SRF signalling. MRTF-A-SRF, in turn, induces malignant progression (Faria et al., 2023). These observations suggest that the progression of TAM-treated ER-Src cells into fully malignant cells involves two main phases. During the first 12 hours of Src activation, cells acquire a phenotypic state akin to premalignant breast cells, characterized by the gain of sustained proliferative abilities through processes involving the transient nucleation of actin filament (F-actin) and an increase in actomyosin contractility in cells that maintain an epithelial-like state. 24 hours after Src activation, cells have progressed into a malignant phase, defined by the loss of epithelial-like organisation associated with the downregulation of Ecad and Pcad and the upregulation of the EMT transcription factor SNAIL1 (Faria et al., 2023; Selvaggio et al., 2020; Tavares et al., 2017). We now provide evidence that the proliferative advantage acquired by premalignant ER-Src cells requires a transient mechanical crosstalk between AJs and FAs. Thus, tensile forces at AJs and FAs may have paradoxical roles during tumour progression. An increase in tensile forces at AJs and FAs could be first required for premalignant breast cells to acquire a proliferative advantage and to set up the conditions enabling their subsequent malignant progression, while the subsequent weakening of forces at AJs and FAs could allow for malignant behaviours.

Results

Src strengthens tensile forces at AJs prior to inducing EMT

Prior to acquiring malignant features, premalignant ER-Src cells turn transiently stiffer (Tavares et al., 2017). Increased cortex tension can promote cytoskeletal anchoring of Ecad at cell–cell contacts, leading to enhanced Ecad clustering and stability (Slovakova et al., 2022). We therefore asked if the transient stiffening state of TAM-treated ER-Src cells was associated with higher tension at AJs. To this end, we generated ER-Src cells stably expressing an Ecad fluorescence resonance energy transfer (FRET)-based tension sensor (Ecad-TS), known to respond to changes in tensile forces at cell-cell contacts (Borghi et al., 2012). The Ecad-TS was built by inserting a tension module (TS), containing a flagelliform elastic linker flanked by the mTFP1 donor and Venus acceptor fluorescent proteins in the Ecad coding sequence, between the transmembrane domain and the catenin-binding domain (Fig. 1A). As expected, the Ecad-TS was recruited at cell-cell contacts where it co-localized with p120ctn (Fig. 1B). To ensure that the Ecad-TS was functional, we tested if expressing the Ecad-TS in MDA-MB-231 cells that lack Ecad (Ribeiro et al., 2010), restored cell-cell contacts. While p120ctn was barely detectable in control MDA-MB-231 cells, those expressing the Ecad-TS recruited p120ctn at the membrane between adjacent Ecad-TS expressing MDA-MB-231 cells and acquired a cobblestone-like shape (Fig. 1C). We next assessed if tensile forces applied to the Ecad-TS were altered during transformation of ER-Src cells by performing fluorescence lifetime measurement (FLIM) of the Ecad-TS donor, a quantitative imaging technique that is less sensitive to imaging or processing artifacts than the FRET ratio-metric approach (Cost et al., 2015; Padilla-Parra and Tramier, 2012; Wallrabe and Periasamy, 2005). For FLIM analysis we focused on donor's lifetimes, which increases as the distance with the acceptor increases. This approach revealed that the donor lifetime of the Ecad-TS was significantly extended in ER-Src cells treated with TAM for 6 or 12 hours, compared to those treated with the vehicle EtOH for the same time (Fig. 1D), suggesting that AJs are under higher tension in premalignant ER-Src cells. While cells undergo EMT 24 hours after TAM treatment (Selvaggio et al., 2020), those that still maintained cell-cell contacts retained an extended donor lifetime of the Ecad-TS (Fig. 1D). To ensure that alterations of the Ecad-TS donor lifetime in TAM-treated cells resulted from higher tensile forces on Ecad, we also generated ER-Src cells expressing a control Ecad-TS construct lacking the βcat–binding domain (Ecad-TSΔcyto), which therefore cannot associate with F-actin (Fig. 1A). Ecad-TSΔcyto localised with p120ctn at cell-cell contacts in ER-Src cells (Fig. 1B), but did not recruit p120ctn at the cell membrane in MDA-MB-231 cells

(Fig. 1C). The donor lifetime of the Ecad-TSΔcyto was not affected between EtOH and TAM-treated cells at any time point (Fig. 1E), indicating that the extended donor lifetime of the Ecad-TS in TAM-treated ER-Src cells depends on its ability to interact with the actin cytoskeleton. The Ecad-TS donor lifetime also depends on Myosin II activity, as Blebbistatin significantly lowered the Ecad-TS donor lifetime in cells treated with EtOH or TAM for 6 hours, compared to those grown in the absence of Blebbistatin (Supp. Fig. 1A).

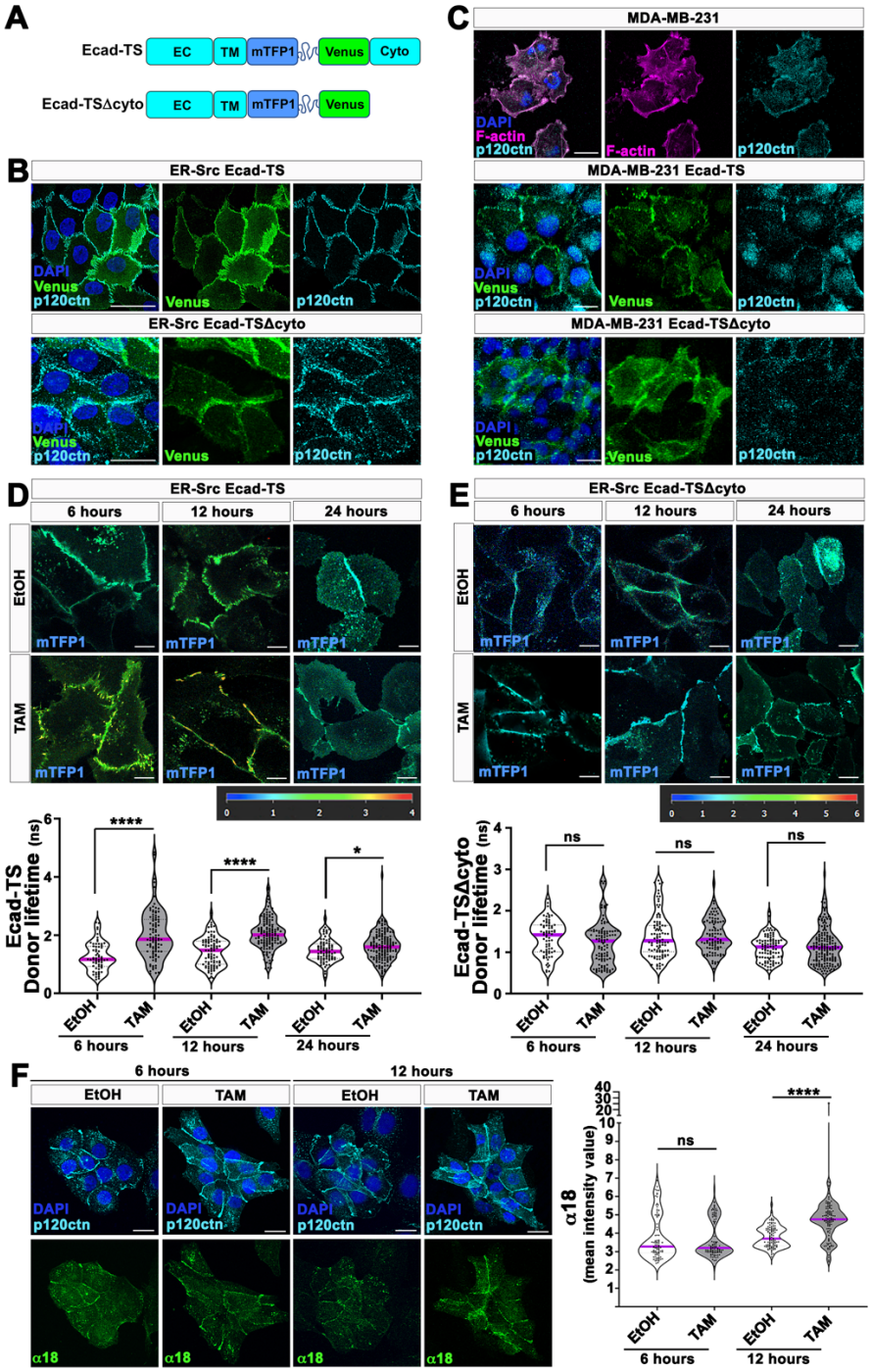

Figure 1: Prior to undergoing EMT, TAM-treated ER-Src cells strengthen tensile forces at AJs. (A) Schematics of the Ecad-TS and Ecad-TSΔcyto, consisting of the mTFP1/Venus

171 FRET pair separated by an elastic linker, inserted between the transmembrane (TM) and
172 cytoplasmic (cyto) domains of Ecad (Ecad-TS). Ecad-TSΔcyto lacks the cytoplasmic domain.
173 EC: extracellular domain. **(B)** Confocal images of ER-Src cells expressing the Ecad-TS (Venus
174 in green) or Ecad-TSΔcyto (Venus in green) and stained with anti-p120ctn (cyan) and DAPI
175 (blue). **(C)** Confocal images of MDA-MB-231 cells, stained with anti-p120ctn (cyan),
176 Phalloidin (magenta) and DAPI (blue) or expressing Ecad-TS (Venus in green) or Ecad-
177 TSΔcyto (Venus in green), and stained with anti-p120ctn (cyan) and DAPI (blue). **(D)** (Top)
178 ER-Src cells expressing Ecad-TS and treated with EtOH or TAM for 6, 12 or 24 hours. Color
179 bar indicates 0–4 ns. (Bottom) Quantification from three biological replicates of the mTFP1
180 lifetime at cell-cell contacts in ER-Src cells expressing the Ecad-TS and treated with EtOH or
181 TAM for 6, 12 or 24 hours. **(E)** (Top) ER-Src cells expressing the Ecad-TSΔcyto and treated
182 with EtOH or TAM for 6, 12 or 24 hours. Color bar indicates 0–6 ns. (Bottom) Quantification
183 from three biological replicates of the mTFP1 lifetime at cell-cell contacts in ER-Src cells
184 expressing the Ecad-TSΔcyto and treated with EtOH or TAM for 6, 12 or 24 hours. Higher and
185 lower donor lifetime correspond to higher and lower tension, respectively. **(F)** (Left) Confocal
186 images of ER-Src cells treated with EtOH or TAM for 6 or 12 hours and stained with the α18
187 antibody (green), anti-p120ctn (cyan) and DAPI (blue). (Right) Quantification from three
188 biological replicates of the α18 mean intensity levels at cell-cell contacts in ER-Src cells treated
189 with EtOH or TAM for 6 or 12 hours. Quantifications are presented as violin plots with the
190 magenta lines indicating median values. Statistical significance was calculated using Mann –
191 Whitney t-tests. ns indicates non-significant. *P<0.05; ****P<0.0001. Scale bars represent 20
192 μm.
193

194 To confirm that prior to disassembling AJs 24 hours after TAM treatment, AJs are under higher
195 tension, we stained cells with an antibody against the α18 epitope of αcat, a cryptic site revealed
196 when tension is applied at AJs (Nagafuchi and Tsukita, 1994). While the intensity of the α18
197 antibody at cell-cell contacts was not significantly different between ER-Src cells treated with
198 EtOH or TAM for 6 hours, it was significantly higher in cells treated with TAM for 12 hours,
199 compared to those treated with EtOH for the same time (Fig. 1F). Because total αcat levels were
200 not affected between EtOH and TAM-treated cells (Supp. Fig. 1B and C), we conclude that AJs
201 are under higher tension in premalignant ER-Src cells, prior cells disassembling AJs.
202

203 **FAs are transiently under higher tension in premalignant ER-Src cells**

204 FAs are mechanically coupled to AJs and to the cortex (Han and de Rooij, 2016; Mui et al.,
205 2016; Zuidema et al., 2020). Moreover, premalignant ER-Src cells accumulate polarised FA-
206 associated stress fibres (Tavares et al., 2017). We therefore asked if tension at FAs was also
207 affected in premalignant ER-Src cells. We generated ER-Src cells expressing a Vinculin tension
208 sensor (Vin-TS), which contains the tension module inserted between the head domain that
209 recruits Vinculin to FAs and the tail domain, which binds to the mechanotransduction force
210 machinery and responds to change in tension at FAs (Grashoff et al., 2010; Humphries et al.,
211 2007; Ziegler et al., 2008). To abrogate the ability of the Vin-TS to respond to tension, we also

generated stable ER-Src cells expressing a Vin-TS lacking the tail domain (Vin-TSΔtail) (Fig. 2A). Vin-TS and Vin-TSΔtail mainly localised with Zyxin at FAs (Fig. 2B). FRET-FLIM analysis indicated that the donor lifetime of the Vin-TS at FAs was slightly extended 6 hours after TAM treatment, compared to those treated with EtOH for the same time. This effect was strongly enhanced 12 hours after TAM-treatment. However, 24 hours after treatment, this differential behaviour was lost between EtOH- and TAM-treated cells (Fig. 2C).

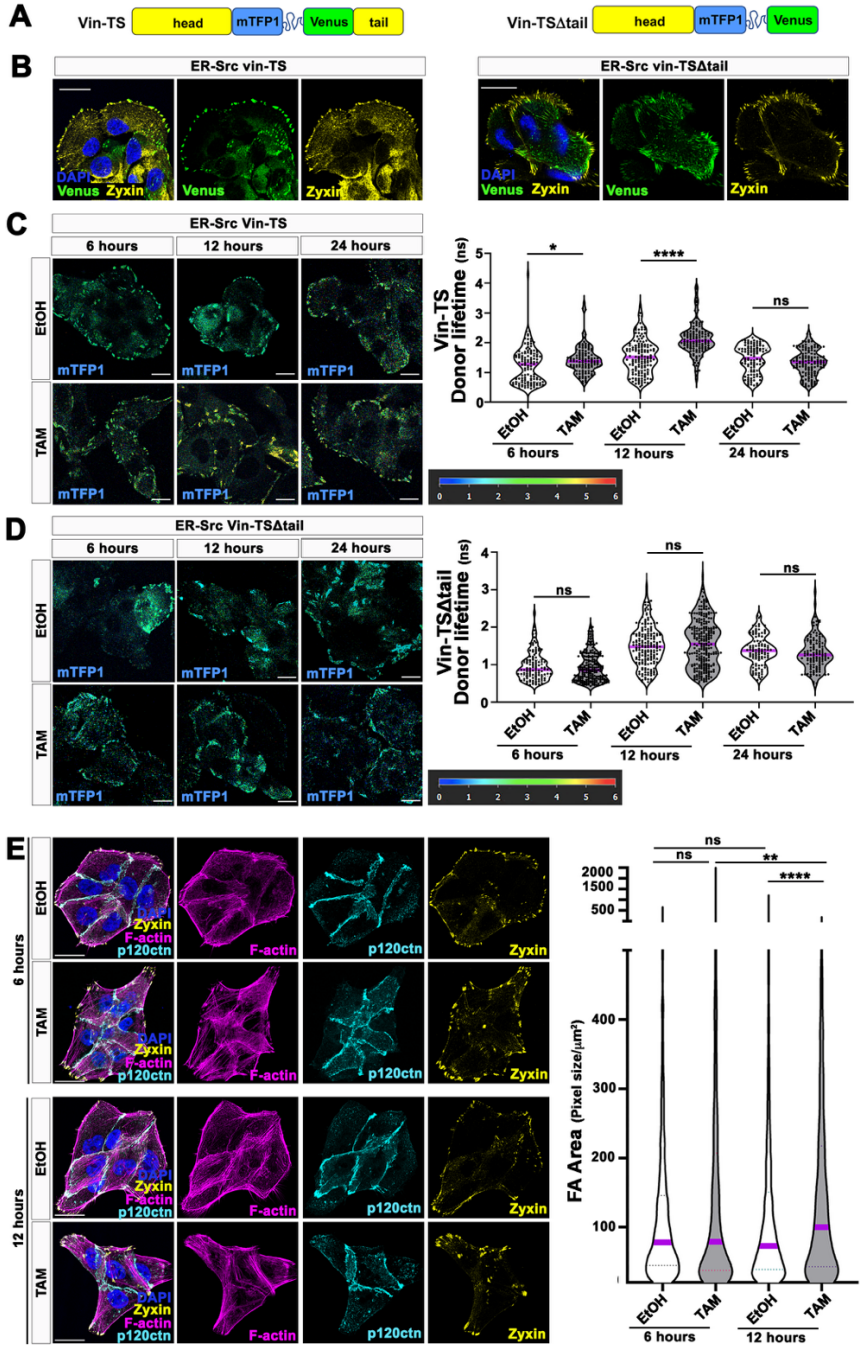

Figure 2: FAs are larger and transiently under higher tension in ER-Src cells. (A) Schematics of the Vin-TS and Vin-TSΔtail, consisting of the mTFP1/Venus FRET pair separated by an elastic linker, inserted between the head and tail domains of Vinculin (Vin-TS). Vin-TSΔtail lacks the tail domain. **(B)** Confocal images of ER-Src cells expressing the

Vin-TS (Venus in green) or Vin-TSΔtail (Venus in green) and stained with anti-Zyxin (yellow) and DAPI (blue). **(C)** (Left) ER-Src cells expressing the Vin-TS and treated with EtOH or TAM for 6, 12 or 24 hours. Color bar indicates 0–6 ns. (Right) Quantification from three biological replicates of the mTFP1 lifetime at FAs in ER-Src cells expressing the Vin-TS and treated with EtOH or TAM for 6, 12 or 24 hours. Higher and lower donor lifetime correspond to higher and lower tension, respectively. **(D)** (Left) ER-Src cells expressing the Vin-TSΔtail and treated with EtOH or TAM for 6, 12 or 24 hours. Color bar indicates 0–6 ns. (Right) Quantification from three biological replicates of the mTFP1 lifetime at FAs in ER-Src cells expressing the Vin-TSΔtail and treated with EtOH or TAM for 6, 12 or 24 hours. **(E)** (Left) Confocal images of ER-Src cells treated with EtOH or TAM for 6, or 12 hours, stained with Phalloidin (magenta) to mark F-actin, anti-Zyxin (yellow) to mark FAs and anti-p120ctn (cyan) to mark AJs. (Right) Quantification from three biological replicates of FA area in ER-Src cells treated with EtOH or TAM for 6 or 12 hours. Quantifications are presented as violin plots with the magenta lines indicating median values. Statistical significance was calculated using Mann – Whitney t-tests. ns indicates non-significant. *P<0.05; **P<0.01; ****P<0.0001. Scale bars represent 20 μm.

In contrast, the donor lifetime inVin-TSΔtail was not altered between EtOH- and TAM-treated cells at any time point (Fig. 2D). Moreover, Blebbistatin reduced the donor lifetime of the Vin-TS 12 hours after EtOH or TAM treatment (Supp. Fig. 2A), indicating that the extended donor lifetime of the Vin-TS in TAM-treated ER-Src cells depends on Myosin II activity.

High tension across Vinculin has been associated with FA enlargement (Grashoff et al., 2010). Thus, to confirm that FAs are under higher tension in premalignant ER-Src cells, we evaluated the size of Zyxin-positive area 6 and 12 hours after EtOH or TAM treatment (Fig. 2E). Quantifications indicated that the average area of Zyxin puncta was significantly larger in ER-Src cells treated with TAM for 12 hours, compared to those treated with EtOH for the same time (Fig. 2E), suggesting that ER-Src cells assemble larger FAs 12 hours after TAM treatment. Together, we conclude that FAs are under higher tension in premalignant ER-Src, prior cells undergoing EMT.

Tension at FAs is required to strengthen forces at AJs in premalignant ER-Src cells

Forces on FAs can be transferred to AJs (Mui et al., 2016; Zuidema et al., 2020). We therefore asked if preventing the transient increase in tension at FAs suppressed the ability of premalignant ER-Src cells to increase tension at AJs. We first tested the effect of inhibiting the activity of FAK, as FAK plays a key role in building up tensile forces at FAs (Wang et al., 2001). Consistent with previous report (Selvaggio et al., 2020), FAK phosphorylation (pFAK) was strongly potentiated after 12 hours of treatment with TAM (Supp. Fig. 3A). Blocking FAK phosphorylation with PF-573228, a known FAK inhibitor (FAKi), strongly reduced pFAK levels in cells treated with either EtOH or TAM for 12 hours, compared to those treated with

DMSO (Supp. Fig. 3A). Inhibiting FAK activity did not prevent the assembly of FAs, seen by the presence of Zyxin and Vin-TS-positive foci in ER-Src cells co-treated with FAKi and EtOH or TAM (Fig. 3A). However, FAK activity is required for strengthening tensile forces at FAs in premalignant cells, as the extended Vin-TS donor lifetime at FAs 12 hours after TAM treatment was suppressed in the presence of FAKi. In contrast, FAKi did not affect the Vin-TS donor lifetime in EtOH-treated cells (Fig. 3B).

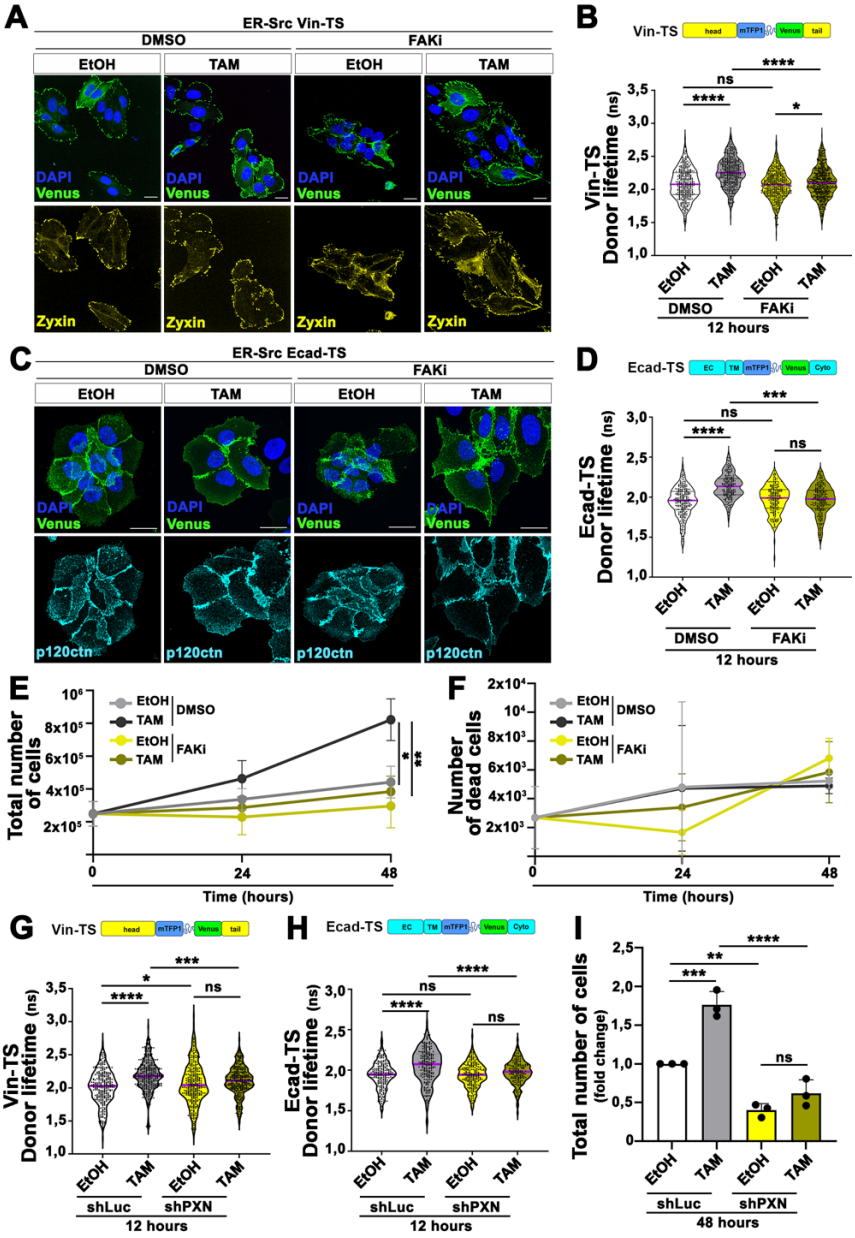

Figure 3: TAM-treated ER-Src cells lose the ability to increase tensile forces at AJs and to grow when unable to strengthen forces at FAs. (A) Confocal images of ER-Src cells expressing the Vin-TS (Venus in green) and co-treated with EtOH or TAM and DMSO or PF-573228 (FAKi) for 12 hours. Cells are stained with anti-Zyxin (yellow) and DAPI (blue). **(B)** Quantification from three biological replicates of the mTFP1 lifetime at FAs in ER-Src cells expressing the Vin-TS and co-treated with EtOH or TAM and DMSO or PF-573228 (FAKi) for 12 hours. **(C)** Confocal images of ER-Src cells expressing the Ecad-TS (Venus in green)

276 and co-treated with EtOH or TAM and DMSO or PF-573228 (FAKi) for 12 hours. Cells are
277 stained with anti-p120ctn (cyan) and DAPI (blue). **(D)** Quantification from three biological
278 replicates of the mTFP1 lifetime at AJs in ER-Src cells expressing the Ecad-TS and co-treated
279 with EtOH or TAM and DMSO or PF-573228 (FAKi) for 12 hours. Quantifications of donor
280 lifetime are presented as violin plots with the magenta lines indicating median values. Scale
281 bars represent 20 µm**. (E)** Growth curve of ER-Src cells co-treated with EtOH or TAM and
282 DMSO or PF-573228 (FAKi) during 48 hours. **(F)** Quantification of dead ER-Src cells co-
283 treated with EtOH or TAM and DMSO or PF-573228 (FAKi) at 24h and 48h timepoints. **(G)**
284 Quantification from three biological replicates of the mTFP1 lifetime at FAs in ER-Src cells
285 expressing the Vin-TS and shLuc or shPXN and treated with EtOH or TAM for 12 hours. **(H)**
286 Quantification from three biological replicates of the mTFP1 lifetime at AJs in ER-Src cells
287 expressing the Ecad-TS and shLuc or shPXN and treated with EtOH or TAM for 12 hours. **(I)**
288 Quantification of the total number of ER-Src cells expressing shLuc or shPXN and treated with
289 EtOH or TAM for 48 hours. Statistical significance was calculated using one-way ANOVA
290 with Tukey's multiple comparison. ns indicate non-significant. *P<0,05; **P<0.01;
291 ***P<0.001; ****P<0.0001.
292

293 We then tested if inhibiting FAK activity affected tension at AJs. ER-Src cells co-treated with
294 FAKi and EtOH or TAM for 12 hours still assembled in clusters with p120ctn and the Ecad-TS
295 localised at the interface between neighbouring cells (Fig. 3C). However, FAKi prevented the
296 extended Ecad-TS donor lifetime at AJs in TAM-treated ER-Src cells at 12 hours (Fig. 3D).
297 Moreover, FAKi significantly suppressed the growth of TAM-treated cells at 48 hours (Fig.
298 3A), but had no major effect on cell viability (Fig. 3F), indicating that FAK activation provides
299 a proliferative advantage to TAM-treated ER-Src cells.
300 To confirm that increased tension at FAs strengthens forces at AJs and is required for cellular
301 transformation, we knocked down PXN using small-hairpin RNAs (shPXN), as Paxillin is one
302 of the consensus FA components, not shared between AJs and FAs (Horton et al., 2016; Mui et
303 al., 2016). EtOH or TAM-treated ER-Src cells expressing shPXN showed reduced Paxillin
304 protein levels, compared to those infected with small-hairpin RNAs against Luciferase (shLuc),
305 used as control (Supp. Fig. 3B). Knocking down PXN in ER-Src cells did not prevent the
306 assembly of Zyxin- and Vin-TS-positive FAs (Supp. Fig. 3C). It did not either induce the loss
307 of cell-cell contacts, as Ecad was still localised between adjacent PXN-depleted cells or
308 between PXN-depleted cells and those expressing Paxillin (Supp. Fig. 3D). However, knocking
309 down PXN suppressed the extended donor lifetime of the Vin-TS (Fig. 3G) and of the Ecad-TS
310 (Fig. 3H) in cells treated with TAM for 12 hours. Moreover, PXN-depleted cells showed a
311 growth impairment, compared to those expressing shLuc (Fig. 3I). Thus, we conclude that the
312 transient strengthening of FAs in premalignant ER-Src cells is required to increase tension at
313 AJs and to sustain cell growth.
314

315 **Premalignant ER-Src cells unable to assemble AJs fail to strengthen tension at FAs.**

316 We then tested if, in turn, tension at AJs was transferred to FAs in premalignant ER-Src cells.
317 To this end, we disrupted cell-cell adhesion using the calcium chelator EGTA, which prevents
318 *trans* junctional homophilic interactions between cadherin extracellular domains (Kartenbeck
319 et al., 1982). Thirty minutes of EGTA treatment was sufficient to induce cell rounding and the
320 loss of cell-cell contacts in ER-Src cells (Supp. Fig. 4A). After removal of EGTA from the
321 media, cells remained viable for at least 24 hours (Supp. Fig. 4B), and recovered a cobblestone-
322 like shape, with p120ctn localised at cell-cell contacts (Supp. Fig. 4A). This shows that the
323 EGTA-dependent loss of cell-cell contacts is reversible. Thus, we first tested if EGTA affected
324 the size of FAs 12 hours after TAM treatment. As expected, ER-Src cells co-treated with EGTA
325 and EtOH or TAM for 12 hours maintained a rounder shape with E-cad poorly recruited at cell-
326 cell contacts, compared to those grown in the absence of EGTA (Fig. 4A). Quantification of
327 the size of Zyxin-positive puncta indicates that EGTA treatment significantly reduced the
328 average area of Zyxin-positive FAs in both EtOH- and TAM-treated cells (Fig. 4B). Thus,
329 tension at AJs could be required to strengthen forces on FAs. Accordingly, FLIM-FRET on the
330 Vin-TS indicates that the extended donor lifetime 12 hours after TAM treatment was
331 suppressed in the presence of EGTA. In contrast, EGTA had no major effect on the Vin-TS
332 donor lifetime in EtOH-treated cells (Fig. 4C). EGTA treatment also prevented the transient
333 increase in cell stiffening 6 hours after TAM treatment (Fig. 4D). Taken together, these
334 observations suggest that higher tension exerted between TAM-treated ER-Src cells through
335 cadherins, reinforces cortical tension and increases tensile forces at FAs.

336

337 **Premalignant ER-Src cells unable to assemble AJs fail to sustain proliferation.**

338 We then tested the consequences of preventing AJ assembly on the ability of TAM-treated ER-
339 Src cells to gain sustained proliferative abilities. Consistent with previous reports (Faria et al.,
340 2023; Tavares et al., 2017), TAM-treated ER-Src cells showed a significant higher number of
341 cells in S-phase of the cell cycle, 12 (Fig. 4E) and 24 (Fig. 4F) hours after treatment, compared
342 to those treated with EtOH for the same time. However, in the presence of EGTA, TAM-treated
343 cells lost their ability to gain self-sufficiency in growth properties, 12 (Fig. 4E) or 24 (Fig. 4F)
344 hours after Src activation. This effect is not due to cell death induced by EGTA, as EGTA-
345 treated cells survived equally well in all experimental conditions (Supp. Fig. 4C, D). EGTA
346 does not suppress the ability of TAM-treated cells to acquire sustained proliferative abilities
347 by preventing Src activation, as the phosphorylation levels of the ER-Src fusion protein (pER-

348 Src) were not significantly different between cells treated with TAM only and those co-treated
349 with TAM and EGTA (Supp. Fig. 4E).

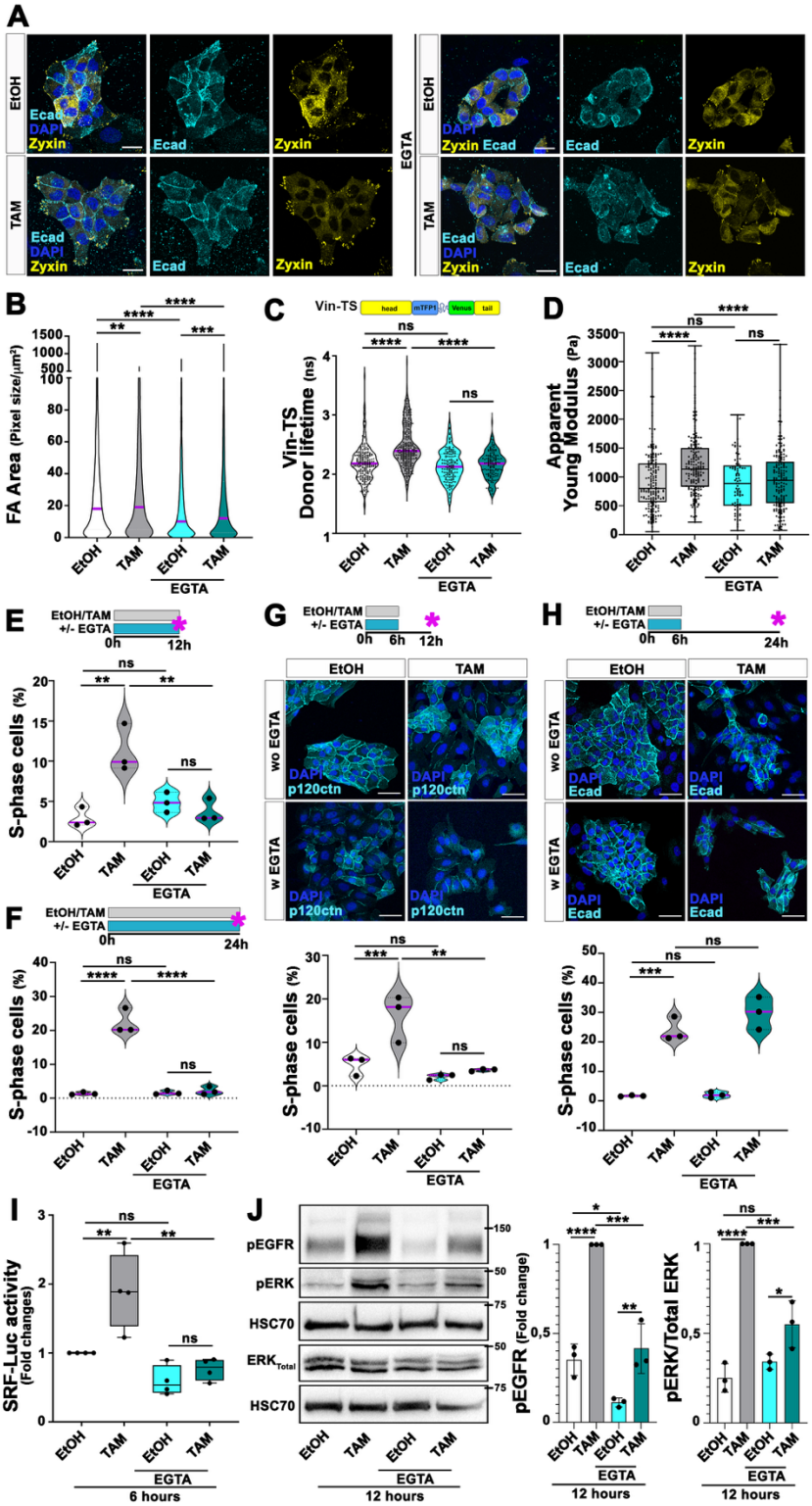

350

351 **Figure 4: EGTA treatment hampers the ability of TAM-treated ER-Src cells to increase**
352 **tension at FAs and to acquire sustained proliferative ability. (A)** Confocal images of ER-
353 Src cells treated with EtOH or TAM in the presence or absence of EGTA for 12 hours, stained
354 with anti-Ecad (cyan) to mark AJs, anti-Zyxin (yellow) to mark FAs and DAPI (blue) to stain
355 nuclei. **(B)** Quantification from three biological replicates of FA area in ER-Src cells treated

356 with EtOH or TAM in the presence or absence of EGTA for 12 hours. **(C)** Quantification from
357 three biological replicates of the mTFP1 lifetime at FAs in ER-Src cells expressing the Vin-TS
358 and treated with EtOH or TAM in the presence or absence of EGTA for 12 hours. **(D)**
359 Quantification from three biological replicates of the Apparent Young's modulus of ER-Src
360 cells treated with EtOH or TAM in the presence or absence of EGTA for 6 to 8 hours. (**E-F)**
361 (Top of each graph) Schematics of the experimental designs. Magenta stars indicate the time
362 points at which cells were collected for cell cycle analysis. (Bottom) Quantification from three
363 biological replicates of the percentage of ER-Src cells in S-phase, in cells treated with EtOH
364 or TAM hours in the presence or absence of EGTA for **(E)** 12 hours or **(F)** 24 hours. **(G)** (Top)
365 Schematics of the experimental designs. Magenta stars indicate the time points at which cells
366 were collected for cell cycle analysis. (Middle) Confocal images of ER-Src cells treated with
367 EtOH or TAM for 6 hours in the presence or absence of EGTA and left to grow for an additional
368 6 hours in the absence of treatment. (Bottom) Quantification from three biological replicates
369 of the percentage of ER-Src cells in S-phase, in cells treated with EtOH or TAM for 6 hours in
370 the presence or absence of EGTA and left to grow for an additional 6 hours in the absence of
371 treatment. **(H)** (Top) Schematics of the experimental designs. Magenta stars indicate the time
372 points at which cells were collected for cell cycle analysis. (Middle) Confocal images of ER-
373 Src cells treated with EtOH or TAM for 6 hours in the presence or absence of EGTA and left
374 to grow for an additional 18 hours in the absence of treatment. Cells are stained with Ecad
375 (cyan) and DAPI (blue). (Bottom) Quantification from three biological replicates of the
376 percentage of ER-Src cells in S-phase, in cells treated with EtOH or TAM for 6 hours in the
377 presence or absence of EGTA and left to grow for an additional 18 hours in the absence of
378 treatment. **(I)** Quantification from three biological replicates of the fold changes in Luciferase
379 activity between ER-Src cells transfected with the SRF-responsive-Luc reporter gene and
380 treated with EtOH or TAM in the presence or absence of EGTA. **(J)** (Left) Western blots on
381 protein extracts from ER-Src cells treated with EtOH or TAM for 12 hours in the presence or
382 absence of EGTA, blotted with anti-pEGFR, anti-pERK and anti-HSC70 used as loading
383 control (middle) or anti-ERK (ERK_{Total}) and anti-HSC70 (bottom). (Right) Quantifications
384 from three biological replicates of pEGFR levels, normalised to HSC70 or the ratio of pERK
385 over total ERK levels, normalised to HSC70 for the conditions indicated. Quantifications are
386 presented as violin plots with the magenta lines indicating median values (B, C and E to H) or
387 as column plots (D, I and J). Statistical significance was calculated using a linear mixed model.
388 ns indicate non-significant. **P<0.01; ***P<0.001; ****P<0.0001. Scale bars indicate 20 µm.
389

390 We then tested if TAM-treated ER-Src cells regain a proliferative advantage after withdrawing
391 EGTA and allowing AJs re-assembly. Cells co-treated with EGTA and TAM or EtOH for 6
392 hours and left to grow in the absence of treatments for another 6 hours did not recover an
393 epithelial-like morphology with membrane-associated p120ctn at cell-cell contacts. In this
394 experimental setting, EGTA still impeded TAM-treated cells to gain proliferative competency
395 (Fig. 4G), with no effect on cell survival (Supp. Fig. 4F). However, 18 hours after withdrawing
396 EGTA and EtOH, cells completely restored an epithelial-like morphology and those that
397 received EGTA and TAM survived equally well and regained the ability to enter S-phase (Fig.
398 4H and Supp. Fig. 4G).
399

400 We then analysed the impact of EGTA treatment on MRTF-A-SRF and ERK activities, as both
401 pathways provide a proliferative advantage to premalignant ER-Src cells (Faria et al., 2023;
402 Tavares et al., 2017). As previously reported (Faria et al., 2023), the activity of a Luciferase
403 reporter controlled by three SRF binding sites (SRF-Luc) was significantly higher in ER-Src
404 cells 6 hours after TAM treatment, compared to those treated with EtOH. Consistent with a role
405 of cell-cell adhesion in enabling premalignant ER-Src cells to gain proliferative abilities, EGTA
406 suppressed the transient increase in SRF-dependent Luciferase activity in TAM-treated cells
407 (Fig. 4I). EGTA also significantly suppressed the higher phosphorylation levels of EGFR
408 (pEGFR) and ERK (pERK) 12 hours after TAM treatment (Fig. 4J). In these cells, ERK
409 phosphorylation is dependent on EGFR activation, as co-treating TAM-treated ER-Src cells
410 with the EGFR inhibitor tyrphostin AG1478 (EGFRi) strongly reduced pEGFR and pERK
411 levels in both EtOH- and TAM-treated cells (Supp. Fig. 5H). Taken together, these observations
412 suggest that higher tensile forces at AJs provide a proliferative advantage to premalignant ER-
413 Src cells through the activation of the EGFR-ERK and MRTF-A-SRF signalling pathways.
414
415 **P-cadherin builds up tension at AJs and FAs in premalignant ER-Src cells**
416 If higher tensile forces exerted between premalignant ER-Src cells through cadherin homophilic
417 interactions are required to strengthen tension at FAs and for cellular transformation, interfering
418 with cadherin function should phenocopy the behaviour of EGTA-treated cells. MCF10A cells
419 express the two classical cadherins Ecad and Pcad (Kumper and Ridley, 2010). According to a
420 role of Pcad-mediated AJ strengthening in cellular transformation, we reported that the transient
421 accumulation of membrane-associated Pcad in premalignant ER-Src cells promotes a boost of
422 MRTF-A-SRF activity, which sustains cell proliferation (Faria et al., 2023). We therefore asked
423 if Pcad builds up tension at AJs and FAs in premalignant ER-Src cells. ER-Src cells transfected
424 with a small interference RNA against Pcad (siPcad) showed a striking decrease of membrane-
425 associated Pcad, compared to those expressing control small interference RNAs (siCTR). Yet,
426 these cells assembled in clusters with Ecad localised at the interface between neighbouring cells
427 (Fig. 5A). Pcad is required to build up tension at AJs in premalignant cells, as the extended
428 donor lifetime of the Ecad-TS in ER-Src treated with TAM for 12 hours was significantly
429 suppressed by expressing siPcad, compared to those expressing siCTR (Fig. 5B). Knocking
430 down Pcad also prevented the transient extended lifetime of the Vin-TS at FAs in ER-Src cells
431 12 hours after TAM treatment (Fig. 5C). In contrast, reducing Pcad function in EtOH-treated
432 cells slightly increased the donor lifetime of the Ecad-TS (Fig. 5B) and Vin-TS (Fig. 5C). We
433 then analysed the effect of Pcad on the activation of EGFR-ERK signalling. ER-Src cells treated

with TAM for 12 hours and expressing siPcad displayed a strong reduction in Pcad, pEGFR and pERK levels, compared to those expressing siCTR (Fig. 5D).

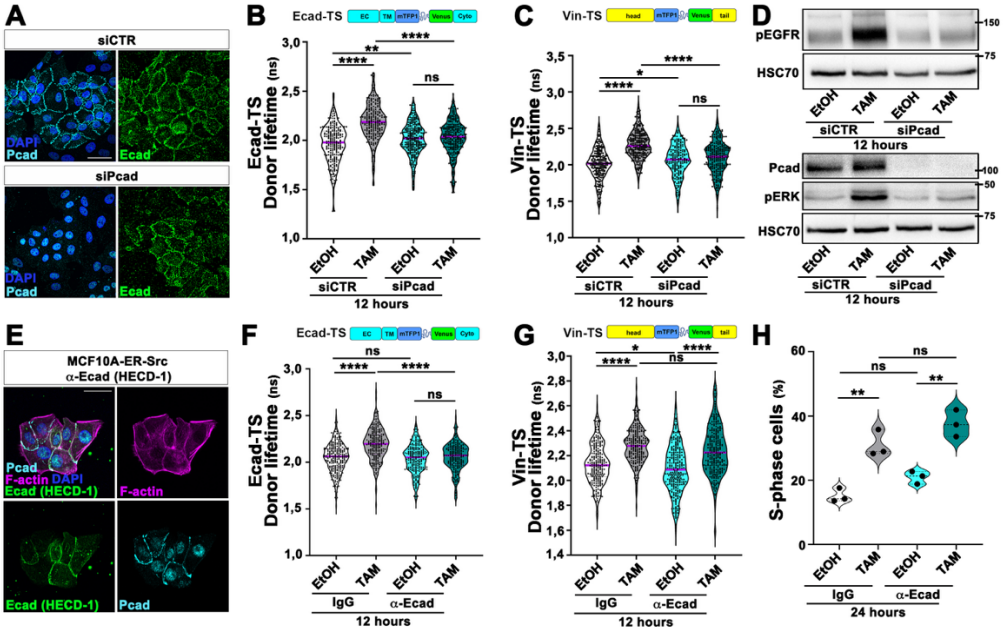

Figure 5: Pcad, but not Ecad, increases tensile forces at AJs and FAs. (A) Confocal images of ER-Src cells expressing siCTR or siPcad, stained with anti-Pcad (cyan), anti-Ecad (green) and DAPI (blue). **(B)** Quantification from three biological replicates of the mTFP1 lifetime at AJs in ER-Src cells expressing the Ecad-TS and siCTR or siPcad and treated with EtOH or TAM for 12 hours. **(C)** Quantification from three biological replicates of the mTFP1 lifetime at FAs in ER-Src cells expressing the Vin-TS and siCTR or siPcad and treated with EtOH or TAM for 12 hours. **(D)** Western blots on protein extracts from ER-Src cells expressing siCTR or siPcad and treated with EtOH or TAM for 12 hours, blotted with anti-pEGFR and anti-HSC70 used as loading control or anti-Pcad, anti-pERK and anti-HSC70. **(E)** Confocal images of ER-Src cells incubated with 10 µg/mL of the Ecad blocking antibody HECD-1 (green), stained with Phalloidin (magenta), anti-Pcad (cyan) and DAPI (blue). **(F)** Quantification from three biological replicates of the mTFP1 lifetime at AJs in ER-Src cells expressing the Ecad-TS and treated with EtOH or TAM in the presence of IgG or Ecad blocking antibody for 12 hours. **(G)** Quantification from three biological replicates of the mTFP1 lifetime at FAs in ER-Src cells expressing the Vin-TS and treated with EtOH or TAM in the presence of IgG or Ecad blocking antibody for 12 hours. **(H)** Quantifications from three biological replicates of the percentage of ER-Src cells in S-phase treated with EtOH or TAM for 24 hours in the presence of IgG or anti-Ecad blocking antibody. Quantifications are presented as violin plots with the magenta lines indicating median values. Statistical significance was calculated using one-way ANOVA with Tukey's multiple comparison. ns indicate non-significant. *P<0,05; **P<0.01; ***P<0.001; ****P<0.0001. Scale bar indicates 20 µM.

We then tested the role of Ecad in increasing tensile forces at FAs and in cellular transformation. Unlike Pcad, the levels of the mature and pro-peptide Ecad forms were not significantly different between cells treated with EtOH and TAM for 12 hours (Supp. Fig, 5). To analyse the consequence of affecting Ecad function on FA strengthening, we blocked the *trans* junctional homophilic interactions between the Ecad extracellular domains using the Ecad blocking

464 antibody HECD-1. As expected, HECD-1 was found associated with the cell membrane. These
465 cells were still assembled in clusters with Pcad localised at the interface between neighbouring
466 cells (Fig. 5E). Although the Ecad blocking antibody prevented the extended donor lifetime of
467 the Ecad-TS in cells treated with TAM for 12 hours (Fig. 5F), it did not suppress the higher
468 Vin-TS donor lifetime in these cells (Fig. 5G), nor their ability to enter S-phase (Fig. 5H). Taken
469 together, we conclude that higher tensile forces at AJs, exerted between TAM-treated ER-Src
470 cells through Pcad homophilic interactions, is required for building up tension at FAs and for
471 ERK-dependent proliferation.
472
473 **Cadherin is required for Src-induced overgrowth *in vivo***
474 We then tested if AJs were required for Src-induced overgrowth *in vivo*. *Drosophila* Ecad
475 (DEcad), encoded by *shotgun*, is the main classical cadherin contributing to cell-cell adhesions
476 in the wing disc epithelium (Wei et al., 2005). We therefore tested if knocking down *DEcad*
477 suppresses the overgrowth of *Drosophila* wing discs overexpressing the *Src oncogene at 64B*
478 *(Src64B)* and the caspase inhibitor *p35* using the UAS-Gal4 system. As expected, distal wing
479 discs overexpressing *Src64B, p35* and two copies of Green Fluorescent Protein (GFP) with the
480 *nubbin*-Gal4 (*nub*-Gal4) driver were bigger than control discs expressing GFP only. Strikingly,
481 replacing one copy of UAS-GFP by a UAS construct expressing double-strand RNA (dsRNA)
482 directed against *Ecad (DEcad-IR#1)* appeared to reduce the growth of *Src/p35*-expressing wing
483 discs (Fig. 6A). Quantification of the ratio between the GFP-positive area and the total wing
484 area for each experimental condition confirmed that knocking down *DEcad* significantly
485 suppressed the overgrowth of *Src/p35*-expressing wing discs (Fig. 6A). Expressing an
486 independent dsRNA against *DEcad (DEcad-IR#2)* also significantly suppressed the overgrowth
487 of *Src64B/p35*-expressing wing discs (Fig. 6B). To confirm that the overgrowth suppression
488 observed reflected indeed a reduction in cell number, we also evaluated the percentage of GFP-
489 positive cells by cell sorting for each experimental condition. While the number of GFP-positive
490 cells was significantly increased by 22% in *nub>Src64B, p35*-expressing wing discs, compared
491 to control discs expressing *GFP* only, knocking down *DEcad* in these tissues restored the
492 percentage of GFP-positive cells to those of control discs expressing *GFP* only (Fig. 6C and
493 Supp. Fig. 6). These observations are in agreement with a role for AJs in Src-induced tissue
494 growth.

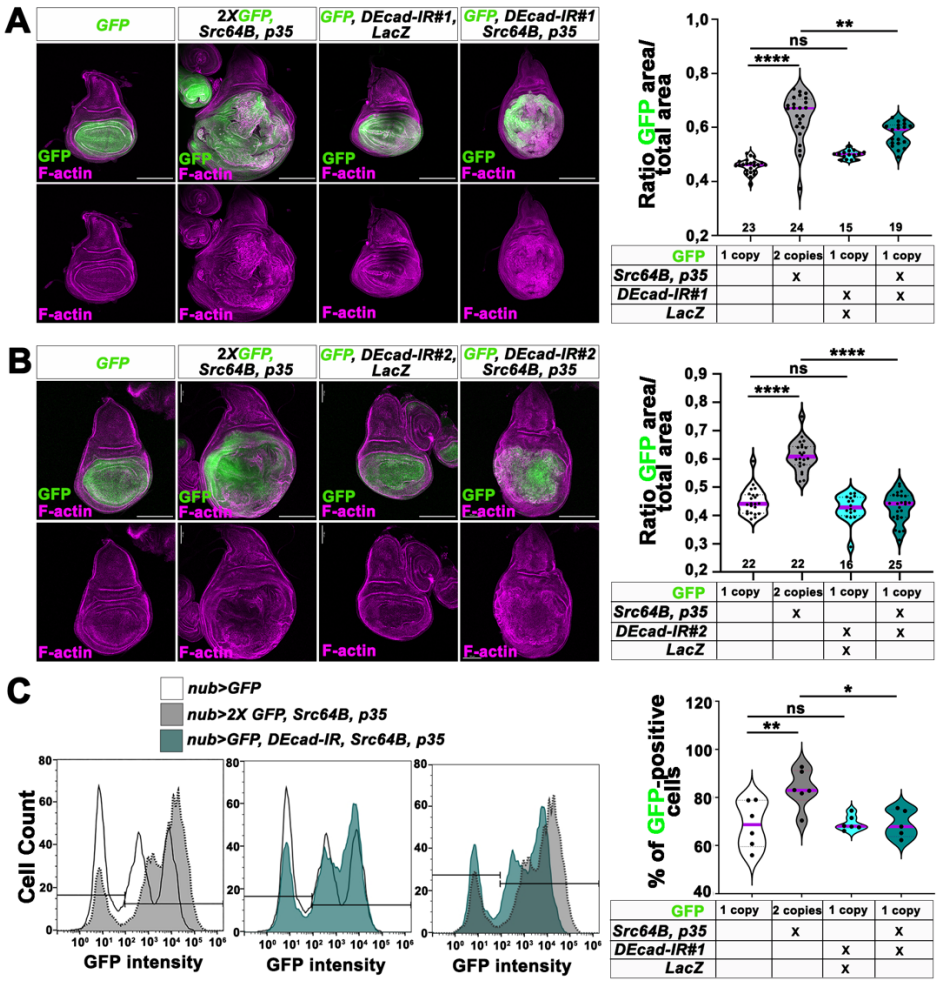

Figure 6: Knocking down *DEcad* suppresses the overgrowth induced by Src overexpression *in vivo*. (A) (Left) Standard confocal sections of third instar wing imaginal discs with dorsal side up, expressing one copy of UAS-CD8::GFP (green) or two copies of UAS-*CD8::GFP* (green), UAS-*p35* and *Src64B*^{UY1332} or one copy of UAS-*CD8::GFP* (green), UAS-*LacZ* and UAS-*DEcad-IR*^{GL00646} or one copy of UAS-*CD8::GFP* (green), UAS- *DEcad-IR*^{GL00646}, UAS-*p35* and *Src64B*^{UY1332} under *nub*-Gal4 control. Discs are stained with Phalloidin (magenta). (Right) Ratio of the *nub>GFP* area over the total wing disc area for the genotypes indicated. Number of samples analysed are indicated on the X axis, and are from two biological replicates. **(B)** (Left) Standard confocal sections of third instar wing imaginal discs with dorsal side up, expressing one copy of UAS-CD8::GFP (green) or two copies of UAS-*CD8::GFP* (green), UAS-*p35* and *Src64B*^{UY1332} or one copy of UAS-*CD8::GFP* (green), UAS-*LacZ* and UAS-*DEcad-IR*^{GD14421} or one copy of UAS-*CD8::GFP* (green), UAS- *DEcad-IR*^{GD14421}, UAS-*p35* and *Src64B*^{UY1332} under *nub*-Gal4 control. Discs are stained with Phalloidin (magenta). (Right) Ratio of the *nub>GFP* area over the total wing disc area for the genotypes indicated. Number of samples indicated on the X axis are from three biological replicates. **(C)** (Left) Histograms of membrane-associated GFP levels in wing discs from the genotypes indicated. (Right) Percentage of GFP-positive cells in wing discs from the genotypes indicated. Quantifications are from five biological replicates. Quantifications are presented as violin plots with the magenta lines indicating median values. Statistical significance was calculated using one-way ANOVA with Tukey's multiple comparison. ns indicate non-significant. **P<0.01; ***P<0.001; ****P<0.0001. Scale bar indicates 20 µM.

517 **Discussion**

518 The weakening of cell-cell and cell-matrix adhesiveness has been proposed to allow cancer
519 cells to acquire hallmarks of malignant tumours, including sustaining proliferative signalling,
520 deregulating cellular metabolism, resisting cell death and activating invasion and metastasis
521 (Bosch-Fortea and Martin-Belmonte, 2018; Sousa et al., 2019). Here, we provide evidence that
522 AJs and FAs have a paradoxical role in premalignant breast epithelial cells overactivating Src.
523 We show that prior to acquiring malignant hallmarks, a transient mechanical crosstalk between
524 Pcad-mediated forces transmission at AJs and FAs is required for ER-Src cells to gain sustained
525 proliferative abilities through activation of the EGFR-ERK and MRTF-A-SRF signalling (Fig.
526 7).

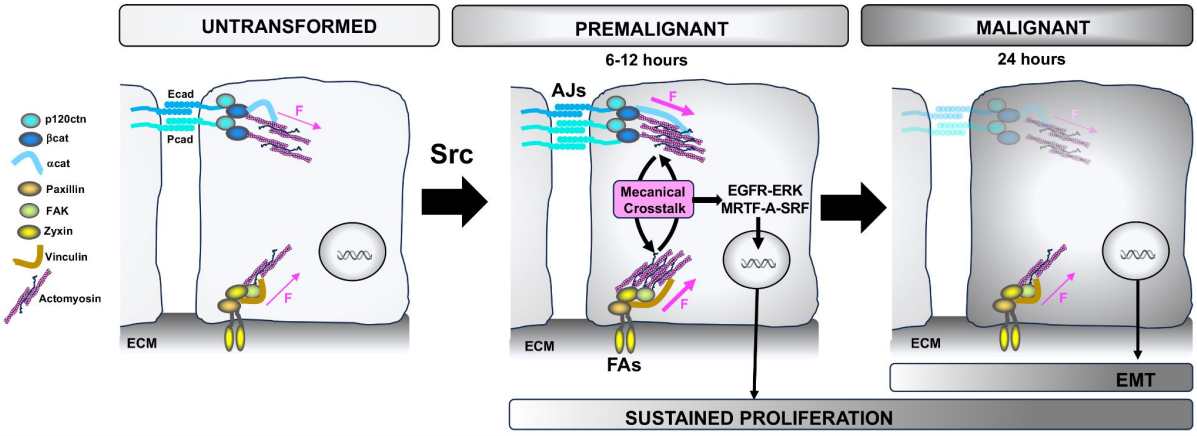

527

528 **Figure 7: Model by which the transient mechanical crosstalk between AJs and FAs in**
529 **premalignant ER-Src cells sustains cell proliferation, prior to undergoing EMT.**
530 Premalignant Src-overactivating MCF10A cells accumulate membrane-associated Pcad, which
531 increases tensile forces at AJs and FAs. In turn, FAs transmit tensile forces to AJs. This positive
532 mechanical crosstalk triggers activation of the EGFR-ERK and MRTF-A-SRF signalling
533 pathways, which provide to TAM-treated ER-Src cells a proliferative advantage. Later during
534 cellular transformation, cells lose membrane-associated Ecad and Pcad, reduce tensile forces
535 at FAs and acquire features associated with EMT.
536

537 Our observations demonstrate that prior to triggering features associated with EMT, oncogenic
538 Src transiently buildups tension at AJs and FAs that are transferred between both adhesion
539 sites. During the first 12 hours of Src activation, Ecad and αcat at AJs and Vinculin at FAs bear
540 higher forces that correlate with the assembly of larger FAs. Moreover, premalignant cells
541 unable to assemble AJs due Ca^{2+} chelation by EGTA or that fail to strengthen tension at AJs
542 due to Pcad depletion, lose the ability to reinforce tension at FAs. Conversely, preventing the
543 strengthening of tensile forces at FAs by restricting FAK or Paxillin activity, suppresses the
544 ability of premalignant ER-Src cells to build up higher tensile forces at AJs. Positive
545 mechanical feedback between AJs and FAs has been reported in other cell types (Sehgal et al.,

546 2018; Zuidema et al., 2020). The strengthening of tensile forces at AJs might constitute a
547 common mechanism preceding EMT. In the *Drosophila* wing disc epithelium, tension at AJs
548 is required in pre-tumoral tissues for subsequent tumour evolution (Montemurro et al., 2025).
549 Likewise, Hepatocyte Growth Factor (HGF) enhances homophilic Ecad interaction in MDCK
550 cells prior to inducing AJ disassembly (de Rooij et al., 2005). EGF also increases the magnitude
551 of tensile force on Ecad in MCF10A cells prior to triggering cell scattering (Rolland et al.,
552 2014). Thus, major alterations in AJs and FAs could constitute prime events in cancer
553 development, ahead of any signs of EMT. Consistent with this possibility, we reported that the
554 two most significant pathways affected in premalignant breast atypical hyperplasia are
555 components of the AJ and FA adhesomes (Tavares et al., 2017).
556
557 We propose that higher tensile stresses at AJs provide a proliferative advantage to Src-
558 overactivating cells by promoting activation of the EGFR-ERK and MRTF-A-SRF signalling
559 pathways. Consistent with this model, TAM-treated ER-Src cells unable to assemble AJs due
560 to EGTA, lose the ability to gain a proliferative advantage and to enhance EGFR-ERK and
561 MRTF-A-SRF signalling activities. In turn, ERK and MRTF-A are required to sustain
562 proliferation in those cells (Faria et al., 2023; Tavares et al., 2017). Moreover, TAM-treated
563 cells regain self-sufficiency in growth capacity if empowered to re-assemble AJs. Furthermore,
564 *in vivo*, DEcad, the sole classical cadherin involved in AJ-dependent cell-cell adhesions,
565 enables the overgrowth of Src-overexpressing wing discs. In agreement with our observations,
566 Myosin II activity is required for ERK-mediated proliferation in premalignant ER-Src cells
567 (Tavares et al., 2017). Moreover, mechanical stress has been shown to activate EGFR-ERK
568 and to trigger MRTF-A nuclear translocation (Chan et al., 2009; Gomez et al., 2010; He et al.,
569 2016; Kuwahara et al., 2010; Somogyi and Rorth, 2004; Yano et al., 2004). Furthermore,
570 mechanical strengths or osmotic stretches applied to MDCK cells triggers cell cycle entry
571 (Benham-Pyle et al., 2015; Narayanan et al., 2020). These extrinsic mechanical stimuli impact
572 on cell proliferation through Ecad-mediated force sensing mechanisms (Benham-Pyle et al.,
573 2015; Mohan et al., 2018; Narayanan et al., 2020). Premalignant ER-Src cells do not require
574 Ecad trans-homophilic interaction to enter S-phase. Rather, this function is endorsed by Pcad,
575 which transiently accumulates at the cell membrane and triggers a boost of MRTF-A-SRF
576 signalling activity (Faria et al., 2023). In addition, we show that Pcad is required to potentiate
577 EGFR-ERK activity in premalignant cells. Pcad also triggers EGFR signalling in oral
578 dysplastic keratinocytes (Lysne et al., 2014). Moreover, in premalignant ER-Src cells, Pcad is
579 necessary to increase tensile forces on Ecad at AJs. Consistent with our observations, Pcad has

been shown to mediate intercellular force transmission in MCF10A cells (Bazellieres et al., 2015). However, in breast cancer cell lines, Pcad has opposite effects, it reduces tension at AJs and destabilises the interaction between Ecad and catenins (Ribeiro et al., 2016; Ribeiro et al., 2013). Pcad overexpression is also strongly associated with cytoplasmic p120ctn accumulation in pancreatic and ovarian cancer cell lines (Cheung et al., 2010; Taniuchi et al., 2005). Thus, Pcad may have a dual opposite effect on AJ strengths that could depend on the stage of tumour progression and therefore on the composition of the AJ adhesomes.

The mechanism by which the Pcad-dependent force transmission activates the EGFR-ERK and MRTF-A-SRF signalling pathways remains to be characterized. Pcad was found to interact with Ecad in MDCK cells (Shafraz et al., 2020). In turn, Ecad interacts with EGFR in mammary epithelial cells and activates the MAPK pathway upon trans-homophilic interaction (Fedor-Chaiken et al., 2003). In keratinocytes, Ecad extracellular engagement leads to the phosphorylation of EGFR at cell-cell contact sites and the ligand-independent activation of the MAPK pathway (Pece and Gutkind, 2000). Yet, Pcad unlikely triggers EGFR phosphorylation solely through Ecad-mediated force transmission, as blocking Ecad homophilic interaction suppresses the higher tensile forces experienced by Ecad in premalignant cells, but not the ability of these cells to enter S-phase. Rather, Pcad-mediated force transmission could cause conformational changes in EGFR at AJs, leading to EGFR homodimerization and ERK activation in an EGF-independent manner. In addition, to provide a proliferative advantage to premalignant ER-Src cells, EGFR activation downstream of Pcad-mediated force transmission may also build up tensile stresses at FAs. In agreement with this model, EGFR activation increases tension on integrin and controls the spatial organization of FAs in Cos-7 cells (Rao et al., 2020). Likewise, in MCF7 cells, EGFR activation increases FAs size and number and integrin-mediated traction forces (Muhamed et al., 2016). Yet, we cannot exclude that Pcad-mediated force transmission affects EGFR-ERK- and MRTF-A-SRF activities through increasing tensile forces at FAs. EGFR has also been shown to interact with integrin in human fibroblasts and endothelial cells and is activated by integrin-mediated adhesions even in the absence of EGF, leading to ERK activation (Moro et al., 1998). ERK is also activated on FA-associated stress fibres in fibroblasts in a myosin II-dependent manner (Hirata et al., 2015). In turn, EGFR signalling can reinforce AJs and junctional actomyosin, as shown in the *Drosophila* ectoderm prior to gastrulation onset (Clarke et al., 2025). Integrin-mediated force transmission can also trigger MRTF-A nuclear translocation (Chan et al., 2009). Moreover, we show that FAK and Paxillin are required for force transmission at FAs in premalignant ER-Src

614 cells, as well as for sustaining cell proliferation. However, as FAK or Paxillin, in turn,
615 strengthens tension at AJs, the growth defect of Src-overactivating ER-Src cells defective for
616 FAK or Paxillin activity could result from the shortfall in AJ strengthening. Forces transmitted
617 from FAs to AJs could further increase tensile forces at AJs, which, upon reaching a certain
618 threshold may trigger the subsequent dissociation of F-actin from AJs and the loss of cell-cell
619 adhesions required for EMT, as proposed in endothelial cells (Kruse and Komarova, 2015).
620 Thus, while uncontrolled growth because of the loss of cell-cell contacts has been proposed to
621 enable the initiation and progression of several types of cancer (Mendonsa et al., 2018), our
622 work reveals that a transient mechanical crosstalk between AJs and FAs in premalignant breast
623 cells could drive tumour growth.

624 **Materials and Methods**

625

626 ***Fly strains and genetics.***

627 Fly stocks used were *nub*-Gal4 (Calleja et al., 1996), Src64B^{UY1332} (Nicolai et al., 2003), UAS-
628 *p35* (Hay et al., 1994), UAS- *DEcad-IR^{GD14421}* (Vienna Drosophila Research Center, VDRC)
629 and UAS-*DEcad-IR^{GL00646}* (Bloomington Drosophila Stock Center). All crosses were
630 maintained at 25 ºC. Male and female larvae were dissected at the end of the third instar.

631

632 ***Cell culture conditions and treatments***

633 The MCF10A-ER-Src cell line (ER-Src for short), kindly provided by K. Struhl (Hirsch et al.,
634 2009), was grown in Complete Growth Media (CGM), composed of DMEM/F12 growth media
635 (Gibco, 11039-047), supplemented with 5% of Charcoal Stripped Horse Serum (CSHS)
636 (Gibco, 16050-122), 20 ng/mL human EGF (Peprotech, AF-100-15), 0.5 µg/mL
637 Hydrocortisone (Sigma, H0888), 100 ng/mL Cholera toxin from Vibrio cholerae (Sigma,
638 C8052), 10 µg/mL Insulin (Sigma, I9278), 0.5 µg/mL Puromycin (Merck, 540411) and 1%
639 Penicilin-Streptomycin (Gibco, 15140). To treat cells with 1 µM 4OH-TAM (Merck, H7904)
640 or EtOH, cells were plated in CGM at 50% confluency and allowed to adhere for 12 to 24
641 hours. Cells were then treated with 1 µM 4OH-TAM (Merck, H7904) or an equal volume of
642 EtOH for the time indicated

643 To analyse the effect of EGTA, cells were plated in CGM at 50% confluency, allowed to adhere
644 for 12 to 24 hours and starved in Restricted Growth Media (RGM), composed of DMEM/F12,
645 supplemented with 0.5% CSHS, 20 ng/mL human EGF, 0.5 µg/mL hydrocortisone, 100 ng/mL
646 cholera toxin, 10 µg/mL insulin, 0.5 µg/mL Puromycin and 1% Penicillin-Streptomycin for 12
647 hours. Cells were then treated with 4 mM EGTA (BioWorld, 40520008) or left without
648 treatment for 30 minutes, and co-treated with 1 µM 4OH-TAM or an equal volume of EtOH
649 for the indicated time. For cell cycle analysis, RGM media without EGF was used.

650 To block the *trans* junctional homophilic interactions between Ecad extracellular domain, cells
651 were seeded and allowed to adhere in the presence of 10 µg/mL of anti-Ecad monoclonal
652 antibody (HECD-1, Invitrogen, 13-1700) or with an identical volume of IgG in CGM. Cells
653 were then starved for 12 hours in RGM lacking EGF in the presence of HECD-1 or IgG and
654 co-treated with 1 µM 4OH-TAM or EtOH and HECD-1 or IgG for 24 hours for cell cycle
655 analysis or directly co-treated with 1 µM 4OH-TAM or EtOH and HECD-1 or IgG in CGM
656 for all other experiments for the time indicated.

657 To inhibit FAK activity, cells were plated in CGM and allowed to adhere for 24 hours. Cells
658 were then treated with 8 μM PF-573228 (Sigma-Aldrich, PZ0117) or DMSO for 12 hours in
659 RGM lacking EGF for cell cycle analysis or for 2 hours in CGM for all other experiments.
660 Cells were then co-treated with EtOH or 1 μM 4OH-TAM and PF-573228 or DMSO for the
661 indicated time in RGM lacking EGF for cell cycle analysis or CGM for all other experiments.
662 To inhibit EGFR activity, cells were seeded in CGM and allowed to adhere for 24 hours. Then,
663 cells were washed twice, grown in DMEM/F12 for 12 hours, and treated with 2 μM of the
664 EGFR inhibitor for 1 hour, and co-treated with 1 μM 4OH-TAM or EtOH in the presence or
665 absence of 2 μM AG1478 (Santa Cruz Biotechnology, sc-200613) for the indicated time.
666 The Human Embryonic Kidney 293T cells (HEK293T) used for viral production were grown
667 in DMEM/F12 supplemented with 10% Fetal Bovine Serum (FBS) Premium heat-inactivated
668 (Thermo Fisher Scientific, 10500-064). MDA-MB-231 cells were grown in Dulbecco's
669 Modified Eagle Medium (DMEM) High Glucose 1X + GlutaMAX™-I (Thermo Fisher
670 Scientific, 31966), supplemented with 10% FBS and 1% Penicillin-Streptomycin (Thermo
671 Fisher Scientific, 15070-063).
672 All cell lines were grown in a humidified incubator at 37 °C, under a 5% CO_2 atmosphere.
673 Tests for mycoplasma contamination were performed every other month, via PCR using the
674 primers MGS0 5′-TGCACCATGTGTCACTCTGTTAACCTC-3′ and GPO1 5′-
675 ACTCCTACGGGAGGCAGCAGTA-3′, which amplify the 16S ribosomal RNA genes of the
676 Mollicutes class of mycoplasma.
677
678 ***Molecular Biology***
679 Ecad-TS and Ecad-TSΔCyto constructs were generated from the canine EcadTSMod sequence
680 kindly provided by Alex Dunn lab (Stanford University) (Borghi et al., 2012). Briefly, the
681 cassette containing the Ecad-TS or Ecad-TSΔCyto was excised with EcoRI and XbaI, and
682 inserted within the pGenLenti vector. Vin-TS and Vin-TSΔtail constructs were generated from
683 the Addgene plasmids #26019 and #26020, kindly provided by Martin Schwartz (Grashoff et
684 al., 2010). Both plasmids were excised from their backbone using the HindIII and SacII
685 restriction enzymes and inserted into the pGenLenti vector.
686
687 ***Lentivirus production and infection***
688 To produce shLuc (Sigma Aldrich, TRCN0000123137), shPXN (Sigma Aldrich,
689 TRCN0000123137), Ecad-TS, Ecad-TSΔcyto, Vin-TS, or Vin-TSΔtail viral particles,
690 HEK293T cells were seeded to reach 70-80% confluency and transfected with 6 μg of pMD2.G

691 (envelope vector), 17 µg of psPAX2 (packaging vector), and 22 µg of plasmids of interest using
692 Lipofectamine 2000 (Thermo Scientific, 11668019). Supernatants were collected 48 and 72
693 hours after transfection, centrifuged at 500 g for 10 minutes, and filtered using a 0.45 µm filter
694 unit to remove large cellular debris, followed by concentration through ultracentrifugation
695 using the Optima L-80 XP Ultracentrifuge (Beckman Coulter) at 32,000 *g* for 1.5 hours at 4ºC.
696 Pellets were resuspended in CGM, aliquoted, and stored at -80ºC. To infect ER-Src cells, plated
697 in 6-well plates, CGM was replaced with 1 mL of CGM supplemented with 10 µg/mL
698 Polybrene® (EMD Millipore, TR-1003-G). Lentiviral particles were added dropwise to each
699 well and mixed by gentle swirling. 12h later, 1 mL of CGM media was added to each well.
700 Cells were incubated for 72 hours and assessed for protein expression by flow cytometry or
701 western blot.
702
703 ***FRET-FLIM Analysis***
704 To perform FRET-FLIM experiments, ER-Src cells stably expressing each FRET-based sensor
705 (Ecad-TS, Ecad-TSΔCyto, Vin-TS, Vin-TSΔtail) were plated on an ibiTreat 8-well chamber
706 slide (Ibidi, 80826) in CGM and allowed to adhere for 24h. After treatment, images were
707 acquired on a single point scanning confocal Stellaris 8, equipped with a fully motorized
708 inverted Leica DMI8 microscope, an HC PL APO 86x/1.20 W motCORR STED white water
709 immersion objective equipped with a correction collar (Leica Microsystems), a WLL, and
710 Falcon and STED modalities, using the Leica LASX software (version 4.6.1.27508). Cells
711 were selected using the acceptor fluorescence signal (EYFP) to ensure the proper localization
712 of the tension sensor (AJs for Ecad-TS and FAs for Vin-TS). The Navigator function on LASX
713 was used to have an overview of the sample and to identify clusters of cells. Fluorescent
714 proteins were excited using a white light laser (WLL) at 85% power, tuned to 80 MHz. The
715 WLL was tuned to 440 or 514 nm to excite mTFP1 and EYFP, respectively, with laser powers
716 of 2% and 2%. Photon detection was performed using two Power HyD X detectors in photon
717 counting (intensity mode), tuned to 440 nm (mTFP1). Images were recorded sequentially by
718 frame scanning unidirectionally at 400 Hz using the galvanometer-based imaging mode, with
719 a line accumulation of 16, and a pixel size of 0.176 µm for an area size of 20,83 µm x 20,83
720 µm (512 x 512, zoom factor of 1, pixel dwell time of 3.1625 µs). For each experiment, a
721 minimum of 20 cell clusters were analysed.
722 FRET detection was based on the time-domain FLIM experiments, which were performed
723 using time-correlated single-photon counting. At least 100 photon events per pixel were

724 collected in all cases, and the lifetime analysis was performed using the Phasor approach on
725 LASX.
726
727 ***Immunofluorescence Analysis***
728 Wing imaginal discs from third instar larvae were dissected in a phosphate buffer at pH 7 (0.1
729 M Na2HPO4, 0.1 M NaH2PO4 at a 72:28 ratio). Discs were then fixed in 4 % formaldehyde
730 in PEM (0.1 M PIPES pH 7, 0.2 mM MgSO4, 1 mM EGTA) for 20 to 30 min, rinsed in
731 phosphate buffer 0.2 % Triton for 15 minutes and incubated 2 hours at 4ºC with Rhodamine-
732 conjugated Phalloidin (Sigma, P-1951) at 0,3 mM in phosphate buffer 0.2 % Triton
733 supplemented with 10 % horse serum. Wing discs were washed 3 times, 10 minutes each,
734 before being mounted in Vectashield (Vector Labs, H-1000). Fluorescence images were
735 acquired on a single point scanning confocal SP5, equipped with a fully motorized inverted
736 Leica DMI6000 microscope, an HC PL APO Lbl. Blue 20x/0.70 IMM objective equipped with
737 a correction collar (Leica Microsystems).
738 For cells, $1.5x10^5$ ER-Src or $1x10^5$ E-cad TS, Vinc-TS, Ecad-TSΔcyt, Vin-TSΔtail cells were
739 seeded on poly-L-lysine-coated coverslips and allowed to adhere for 12 to 24 hours. After
740 treatment, cells were rinsed with PBS 1X and fixed with 4% formaldehyde methanol-free
741 (Thermo Fisher Scientific, 28908) in H_2O, supplemented with 0.06 M PIPES pH 6.8, 0.03 M
742 HEPES pH 7.0, 0.01 M EGTA pH 6.8, and 0.004 M $MgSO_4$ for 10 minutes. Cells were
743 permeabilized with PBS containing 0.1% Triton-X-100 (PBS-T) for 2 minutes at RT and
744 blocked with a blocking buffer (10% FBS in PBS-T) for 1 hour at RT. Rat anti-α18 (1:50; a
745 gift from Professor Akira Nafaguchi, Japan, (Nagafuchi and Tsukita, 1994), mouse anti-
746 p120ctn (1:50; BD Bioscience, 610133), rabbit anti-Zyxin (1:50; Sigma, HPA004835), mouse
747 anti-Ecad (1:50; Invitrogen, 13-1700), mouse anti-Pcad (1:50; BD Bioscience, 610228), rabbit
748 anti-Ecad (1:50; Cell Signalling, 3195) and mouse anti-Paxillin (1:50 or 1:200; BD Bioscience,
749 610051) were incubated overnight at 4ºC in blocking buffer. Coverslips were washed with PBS
750 1X three times for 5 minutes at RT and incubated with FITC-conjugated Donkey anti-Rat IgG
751 (1:200; Jackson ImmunoResearch, 712-095-150), FITC-conjugated Donkey anti-Mouse IgG
752 (1:200; Jackson ImmunoResearch, 715-095-150), Alexa Fluor 647-conjugated Donkey anti-
753 Mouse IgG (1:200; Jackson ImmunoResearch, 715-605-151), CyTM5-conjugated Donkey
754 anti-Rabbit IgG (1:200; Jackson ImmunoResearch, 711-175-152), and Rhodamine-conjugated
755 Phalloidin (Sigma-Aldrich, P-1951) at 0.3 mM in blocking buffer for 1 hour at RT in the dark.
756 After three washes with PBS 1X for 5 minutes, cells were stained with DAPI (1:500; Sigma,
757 D9542) for 5 minutes at RT, washed with PBS 1X for 5 minutes, and mounted in Vectashield.

758 Images were obtained on a single-point scanning confocal Leica SP5, coupled to a Leica
759 DMI6000, using the 63x/1.4 HCX PL APO CS oil immersion objective or with a spinning disk
760 confocal Andor BC43 benchtop system (Oxford Instruments/Andor) using the 60x/1.42 oil
761 immersion objective. Image processing was performed using Imaris version 10.2 or NIH
762 Fiji/ImageJ (Schindelin et al., 2012; Schneider et al., 2012).
763
764 ***Immunoblotting Analysis and Quantification***
765 $2.65x10^5$ ER-Src cells in CGM were plated in a T25 flask. After 6 or 12 hours of treatment,
766 cells were trypsinized with TrypLE™ Express (Gibco, 12604-021) and collected into 1.5 mL
767 tubes. Proteins were extracted by resuspending the cell pellets in Lysis Buffer SDS-Free,
768 composed of 0.05M Tris-HCl pH 7.5 (VWR, 33621.260), 0.15 M NaCl (Sigma-Aldrich,
769 31434), 0.001 M EDTA pH 8.0 (Sigma-Aldrich, E5134), 0.001 M EGTA pH 7.0 (Sigma-
770 Aldrich, E3889), 1% Triton X-100 (Sigma-Aldrich, T8787) and supplemented with 1%
771 protease inhibitors (Sigma-Aldrich, 5892791001) and 1% phosphatase inhibitors (Sigma-
772 Aldrich, 4906845001) on ice for 30 minutes. Samples were centrifuged at 4°C for 30 minutes
773 at 14,000 rpm, and protein was quantified using the Bradford method. For pERK and pEGFR
774 detection, $1.5x10^5$ ER-Src cells were plated in 6-well plates. After 12 hours of treatment, Lysis
775 Buffer SDS-Free, containing 1% protease inhibitors (Sigma-Aldrich, 5892791001) and 1%
776 phosphatase inhibitors (Sigma-Aldrich, 4906845001; Sigma-Aldrich, S6508; Sigma-Aldrich,
777 S7920), was added to cells. Cells were detached using a cell scraper and collected into 1.5 mL
778 tubes. Samples were centrifuged at 4°C for 30 minutes at 14,000 rpm, and protein was
779 quantified using the Bradford method. Laemmli buffer was added to protein samples to a final
780 concentration of 1X, and extracts were boiled for 5 minutes at 95°C, centrifuged for 10 minutes
781 at 8,000 rpm before being resolved by SDS-PAGE electrophoresis and transferred to a 0.45
782 μM PVDF blotting membrane (Amersham, 10600023). Membranes were blocked with 5%
783 BSA in TBS containing 0.1% Tween 20 for 1 hour, cut to separate proteins migrating at diverse
784 molecular weights and incubated with rat anti-α18 (1:1,000; (Nagafuchi & Tsukita, 1994)),
785 rabbit anti-αcat (1:1,000; Thermo Fisher Scientific, MA5-14986), mouse anti-HSC70 (1:8,000;
786 Santa Cruz Biotechnology, sc-7298), mouse anti-Paxillin (1:10,000; BD Bioscience, 610051),
787 mouse anti-phospho-p44/42 MAPK (1:1,000; Cell Signaling, 9106), rabbit anti-p44/42 MAPK
788 (1:2,000; Cell Signaling, 9102), rabbit anti-GAPDH (1:5,000; Sigma, G9545), rabbit anti-
789 pEGFR (1:1,000; Thermo Fisher Scientific, 44-788G) mouse anti-Pcad (1:2,500; BD
790 Bioscience, 610228), rabbit anti-pFAK (pY397) (1:1,000; Cell Signalling), rabbit anti-Ecad
791 (1:1,000; Cell Signalling, 3195) and rabbit anti-phospho Src (pY418) (1:3,000; Invitrogen, 44-

792 660G) diluted in TBS 0.1% Tween 20 supplemented with 3% BSA. Secondary antibodies used
793 were horseradish peroxidase (HRP)-conjugated AffiniPure donkey anti-mouse IgG (1:5,000;
794 Jackson ImmunoResearch, 715-035-150), HRP-conjugated AffiniPure donkey anti-rabbit IgG
795 (1:5,000; Jackson ImmunoResearch, 715-035-152), goat anti-rat IgG-HRP (1:5,000; Santa
796 Cruz biotechnology, sc-2006), IRDye® 680RD-conjugated donkey anti-mouse IgG (1:20,000;
797 LI-COR Bioscences, 926-68072) and IRDye® 800CW-conjugated donkey anti rabbit IgG
798 (1:20,000; LI-COR Bioscences, 926-32213), all diluted in TBS 0.1% Tween 20 supplemented
799 with 1% BSA. Immobilon Western Chemiluminescent HRP substrate (Millipore, P90719) was
800 utilized for detection and visualization in ChemiDoc (Bio-Rad) or Odyssey® M (LI-COR
801 Biosciences) imaging systems. Image Lab (Bio-Rad) and Image Studio (LICOR) software were
802 used for quantification. The intensity levels of each band were normalized to those of the
803 respective control for protein extracts loaded on the same gel for each experimental condition.
804
805 ***Transfections and dual Luciferase Renilla reporter assay***
806 To test the effect of knocking down Pcad, $1.5x10^5$ ER-Src cells resuspended in 2 mL of CGM
807 were plated in 6-well plates for immunoblot analysis or in ibiTreat 8-well chamber slide for
808 FRET-FLIM analysis. After 12 to 24 hours, cells were transfected with 50 nM or 100nM siCTR
809 (Qiagen, 1027310) or 50 nM or 100nM siCDH3 (Qiagen, 1027416, GeneGlobe
810 ID:SI02663941) for FRET-FLIM and immunofluorescence or for immunoblot analysis,
811 respectively, using Lipofectamine 2000, according to the manufacturer's instructions. After 24
812 hours, transfected cells were incubated for another 12 hours in CGM containing EtOH or 4OH-
813 TAM for FRET-FLIM or immunofluorescence analysis. For immunoblot analysis, 12 hours
814 after transfection, the medium was replaced by RGM lacking EGF. After 36 hours, cells were
815 treated with 4OH-TAM or EtOH for the indicated time. To test the effect of EGTA on the
816 activity of the SRF-Luc reporter, $1x10^5$ cells resuspended in 2 mL of CGM were plated in 6-
817 well plates. 12 to 24 hours later, cells were transfected with 0.720µg p3D.A-Luc and 1.44 µg
818 pRL-TK plasmids (Posern et al., 2002) using Lipofectamine 2000, according to the
819 manufacturer's instructions. Cells were then incubated with EGTA for 30 minutes, and co-
820 treated with 4OH-TAM or EtOH in the presence or absence of EGTA for 6 hours in RGM
821 lacking EGF. After trypsinization with TrypLE™ Express (Thermo Fisher Scientific,
822 12604021), cell pellets were resuspended in 250 µL 1× passive lysis buffer (Promega, E1941)
823 and stored overnight at −20°C. Luciferase assay was performed using a Dual-Luciferase
824 Reporter Assay system (Promega, PROME19600010) according to the manufacturer's
825 instructions. Briefly, 100 µL Luciferase assay reagent II (LARII) was added to 80 µL of lysed

826 samples in a 96-well plate. Firefly luminescence was detected using Synergy Mx (BioTek).
827 Then, 100 µL 1X Stop and Glo solution (Promega, PROME19600010) was added to detect
828 Renilla luminescence. Each sample was evaluated in triplicate.
829
830 ***Cell Cycle Profile***
831 For cell cycle analysis, cells treated for 12 or 24 hours were trypsinized with TrypLE™ Express
832 and collected into 5 mL round-bottom polystyrene tubes (Corning, 352235). Cells were
833 centrifuged for 5 minutes at 1,000 rpm at 4ºC, washed with 1 mL of FACS Buffer (PBS 1X
834 supplemented with 2% heat-inactivated FBS (Biowest, S181BH)), centrifuged for 5 minutes at
835 1,000 rpm at 4ºC and resuspended in 500 µL FACS Buffer. Cells were fixed with 1.5 mL 70
836 % Ethanol, added drop-by-drop, while gently vortexed, followed by a 30 minutes incubation
837 at 4ºC. After 5 minutes centrifugation at 2,000 rpm at 4ºC, cells were resuspended in 3 mL of
838 ice-cold PBS 1X, incubated 30 minutes on ice, pelleted again by centrifugation for 5 minutes
839 at 2,000 rpm at 4ºC and resuspended in 300 µL of PBS 1X, supplemented with 100 µg/mL
840 RNAse A (Qiagen, 19101) and 20 µg/mL Propidium Iodide (Sigma, P4170). Samples were
841 incubated for 30 minutes in a 37ºC water bath in the dark. Flow Cytometry was performed at
842 a low flow rate using a BD Accuri C6 Flow Cytometer (Becton-Dickinson, Franklin Lakes,
843 NJ, USA). Cell Cycle profiles were analysed using FlowJo 10.7.1 software (Tree Star, Inc.,
844 Ashland, OR, USA) Cell Cycle platform, using the Watson Model.
845
846 ***Quantification of cell number***
847 To quantify cell number, cells were trypsinized with TrypLE™ Express, washed twice with
848 PBS 1X, and resuspended in PBS 1X. Then, cell suspension was mixed with trypan blue in a
849 1:1 proportion, pipetted into a disposable Countess cell counting chamber slide (Thermo Fisher
850 Scientific, C10228) and cell number was quantified using the Countess 3 Automated Cell
851 Counter (Thermo Fisher Scientific).
852
853 ***Flow Cytometry***
854 To quantify GFP-expressing cells in wing imaginal discs, 25 discs were dissected for each
855 genotype in ice-cold PBS 1X. Samples were then incubated in 200 µL of TrypLE™ for 45
856 minutes at 37°C to facilitate cell dissociation. Mechanical pipetting was performed to ensure
857 complete dissociation before inactivating the TrypLE™ with 200 µL of PBS 1X supplemented
858 with 1% FBS. Cells were centrifuged at 3,500 rpm for 8 minutes, fixed in 500 µL of ice-cold
859 70 % Ethanol, and stored at 4°C. Before analysis, cells were resuspended in 400 µL of PBS

860 1X, and filtered into 5 mL FACS round-bottom tubes. 100 µL of cell suspension was analyzed
861 with medium flow rate settings on a BD Accuri C6 Plus. A description of the gating strategy
862 can be found in Supplementary Figure 6. To confirm the expression of the FRET-tension
863 sensors, transduced ER-Src cells were washed and resuspended in PBS 1X supplemented with
864 0.2% BSA and 0.1% NaN3, at a concentration of $1x10^6$ cells/ml. Cytometric analysis was
865 performed using a FACSCanto II or LSRFortessa flow cytometers (BD), with FACS Diva
866 software.
867
868 ***Atomic force microscopy***
869 $1x10^5$ cells in 2 mL of CGM were plated in a glass bottom dish (World Precision Instruments,
870 FD35-100). 6 hours after treatment with EtOH or TAM in the absence or presence of EGTA,
871 RGM was replaced by CO_2-independent media (Thermo Fisher Scientific 18045054) with
872 EtOH or 4OH-TAM in the presence or absence of EGTA. EGTA induced the appearance of
873 two morphologically distinct cell populations in both EtOH- and TAM-treated cells. The round
874 cell populations were excluded from the analysis, as we assume that these cells are losing
875 adherence to the glass substrate. For the AFM indentation experiments, a Nanowizard 4 (JPK
876 Instruments, Berlin) mounted on top of a light microscope (Zeiss Axiobserver) was used,
877 combined with a petri dish heater to keep the temperature at 37°C during experiments. Arrow-
878 T1 cantilevers (Nanoworld, Neuchatel, Switzerland) were modified with polystyrene beads
879 (radius 2.5 µm, Microparticles GmbH, Berlin, Germany) using epoxy glue to obtain a well-
880 defined spherical indenter geometry and decrease local strain during indentation. The
881 cantilever was lowered over the central part of the cell with a speed of 5 µm s^{-1} until a relative
882 set point of 2.5 nN was reached. Each cell was probed three times in the same location. The
883 resulting force-distance curves were analysed using JPK image processing software (JPK
884 instruments). Force-distance data were corrected for the tip sample separation and fitted with
885 a Hertz model for a spherical indenter to extract the apparent Young's Modulus within an
886 indentation depth of approximately 1 µm. A Poisson ratio of 0.5 was assumed. The average of
887 the Young's Modulus of the three curves was calculated for each cell. A 2-hour time window
888 was required for measurement of the four experimental conditions.
889
890 ***Quantifications***
891 The NIH Fiji/ImageJ program was used to quantify the ratio of the GFP-positive wing disc area
892 to the total disc area. Comparisons between wing imaginal discs overexpressing Src64B and

893 p35 alone or together with UAS-Ecad-IR were performed using the same number of UAS
894 transgenes. For each wing disc, the area of the GFP domain and the area of the whole disc
895 domain highlighted by Phalloidin staining were outlined manually and measured using the
896 *Area* function, which evaluates size in square pixels. The ratio was calculated for each disc
897 between the two. To quantify the intensity of the α18 staining, maximum intensity Z-
898 projections of the p120ctn and α18 channels were performed for each field using the NIH
899 Fiji/ImageJ program. The segmented line tool was used to overlap the p120ctn signal with the
900 line width set to 10. Each line was then used to measure the mean gray value in the α18 channel.
901 Three fields per condition were quantified for each biological replicate. To quantify FA size,
902 maximum intensity Z-projections of the Zyxin channel were performed for each field using the
903 NIH Fiji/ImageJ program. Images were then segmented using the LABKIT Fiji plugin (Arzt et
904 al., 2022) to generate binary masks. The size of particles was then extracted and displayed in
905 pixel units. To compare the size of FAs between ER-Src cells treated with EtOH or TAM for
906 6 or 12 hours, images were acquired on a single point scanning confocal SP5, equipped with a
907 fully motorized inverted Leica DMI6000 microscope (Leica Microsystems), with a 63x
908 objective using a zoom factor 3 to analyse FA area between ER-Src cells treated with EtOH or
909 TAM for 6 or 12 hours or a zoom factor 2 to determine the effect of EGTA on the FA area. 3
910 to 5 fields per condition were quantified for each biological replicate. To analyse FA area
911 between ER-Src cells treated with EtOH or TAM for 6 or 12 hours, particles smaller than 20
912 pixels were considered nonspecific signals and were excluded. To analyse the effect of EGTA
913 on the FA area, all particles were included. R was used for the statistical analysis of AFM data.
914 GraphPad Prism (10.0) was used for all other statistical analysis and for data presentation.

Acknowledgements

Stocks obtained from the Bloomington Drosophila Stock Center (NIH P40OD018537) and from the Vienna Drosophila Research Center, VDRC, were used in this study. We specially thank K. Struhl, Alex Dunn, G. Posern, A. Nagafuchi, A. Dunn and M. Schwartz for reagents and all members of F.J. lab for helpful discussions. We acknowledge the Cell Culture and Genotyping, the Genomics, the Translational Cytometry, the Bioimaging and the Advanced Light Microscopy platforms at i3S.

Competing interests

The authors of this manuscript declare that they have no conflict of interest and no competing financial interests in relation to the work described. The material of this work is original research.

Funding

This research was funded by Fundação para a Ciência e Tecnologia I.P. (FCT) by grant number PTDC/BIA-BFS/0812/2021 to F.J. and PhD fellowship number 2022.11122.BD (doi https://doi.org/10.54499/2022.11122.BD) to L.F. The i3S Bioimaging and Advanced Light Microscopy scientific platforms are both members of the national infrastructure PPBI-Portuguese Platform of BioImaging (POCI-01-0145-FEDER-022122).

Data availability

Original data are available upon request.

Author contributions

Conceptualization F.J.; Methodology F.J., M.A., P.S., A.T.; Investigation, L.F., C.G., I.F.; C.S.L; V.R., S.T., V.M., F.J.; Formal Analysis, L.F., C.G., I.F.; C.S.L; V.R., S.T., V.M., F.J.; Writing – Original Draft, F.J.; Writing – Review & Editing, L.F., C.G., I.F.; C.S.L; V.R., S.T., V.M., F.J.; Funding Acquisition, F.J.; Supervision, F.J., A.T. and L.F.

References

Allred, D. C., Mohsin, S. K. and Fuqua, S. A. (2001). Histological and biological evolution of human premalignant breast disease. *Endocr Relat Cancer* **8**, 47-61.

Allred, D. C., Wu, Y., Mao, S., Nagtegaal, I. D., Lee, S., Perou, C. M., Mohsin, S. K., O'Connell, P., Tsimelzon, A. and Medina, D. (2008). Ductal carcinoma in situ and the emergence of diversity during breast cancer evolution. *Clin Cancer Res* **14**, 370-378.

Angulo-Urarte, A., van der Wal, T. and Huveneers, S. (2020). Cell-cell junctions as sensors and transducers of mechanical forces. *Biochim Biophys Acta Biomembr* **1862**, 183316.

Arpino, G., Laucirica, R. and Elledge, R. M. (2005). Premalignant and in situ breast disease: biology and clinical implications. *Ann Intern Med* **143**, 446-457.

Arzt, M., Deschamps, J., Schmied, C., Pietzsch, T., Schmidt, D., Tomancak, P., Haase, R. and Jug, F. (2022). LABKIT: Labeling and Segmentation Toolkit for Big Image Data. *Front Comp Sci-Switz* **4**.

Bazellieres, E., Conte, V., Elosegui-Artola, A., Serra-Picamal, X., Bintanel-Morcillo, M., Roca-Cusachs, P., Munoz, J. J., Sales-Pardo, M., Guimera, R. and Trepat, X. (2015). Control of cell-cell forces and collective cell dynamics by the intercellular adhesome. *Nat Cell Biol* **17**, 409-420.

Benham-Pyle, B. W., Pruitt, B. L. and Nelson, W. J. (2015). Cell adhesion. Mechanical strain induces E-cadherin-dependent Yap1 and beta-catenin activation to drive cell cycle entry. *Science* **348**, 1024-1027.

Borghi, N., Sorokina, M., Shcherbakova, O. G., Weis, W. I., Pruitt, B. L., Nelson, W. J. and Dunn, A. R. (2012). E-cadherin is under constitutive actomyosin-generated tension that is increased at cell-cell contacts upon externally applied stretch. *Proc Natl Acad Sci U S A* **109**, 12568-12573.

Bosch-Fortea, M. and Martin-Belmonte, F. (2018). Mechanosensitive adhesion complexes in epithelial architecture and cancer onset. *Curr Opin Cell Biol* **50**, 42-49.

Buckley, C. D., Tan, J., Anderson, K. L., Hanein, D., Volkmann, N., Weis, W. I., Nelson, W. J. and Dunn, A. R. (2014). Cell adhesion. The minimal cadherin-catenin complex binds to actin filaments under force. *Science* **346**, 1254211.

Buyuk, B., Jin, S. and Ye, K. (2022). Epithelial-to-Mesenchymal Transition Signaling Pathways Responsible for Breast Cancer Metastasis. *Cell Mol Bioeng* **15**, 1-13.

Calleja, M., Moreno, E., Pelaz, S. and Morata, G. (1996). Visualization of gene expression in living adult Drosophila. *Science* **274**, 252-255.

Carisey, A., Tsang, R., Greiner, A. M., Nijenhuis, N., Heath, N., Nazgiewicz, A., Kemkemer, R., Derby, B., Spatz, J. and Ballestrem, C. (2013). Vinculin regulates the recruitment and release of core focal adhesion proteins in a force-dependent manner. *Curr Biol* **23**, 271-281.

Chan, M. W., Arora, P. D., Bozavikov, P. and McCulloch, C. A. (2009). FAK, PIP5KIgamma and gelsolin cooperatively mediate force-induced expression of alpha-smooth muscle actin. *J Cell Sci* **122**, 2769-2781.

Cheung, L. W., Leung, P. C. and Wong, A. S. (2010). Cadherin switching and activation of p120 catenin signaling are mediators of gonadotropin-releasing hormone to promote tumor cell migration and invasion in ovarian cancer. *Oncogene* **29**, 2427-2440.

Clarke, D. N., Miller, P. W. and Martin, A. C. (2025). EGFR-dependent actomyosin patterning coordinates morphogenetic movements between tissues in Drosophila melanogaster. *Dev Cell* **60**, 270-287 e276.

991 **Cost, A. L., Ringer, P., Chrostek-Grashoff, A. and Grashoff, C.** (2015). How to Measure
992 Molecular Forces in Cells: A Guide to Evaluating Genetically-Encoded FRET-Based
993 Tension Sensors. *Cell Mol Bioeng* **8**, 96-105.
994 **de Rooij, J., Kerstens, A., Danuser, G., Schwartz, M. A. and Waterman-Storer, C. M.**
995 (2005). Integrin-dependent actomyosin contraction regulates epithelial cell scattering.
996 *J Cell Biol* **171**, 153-164.
997 **Faria, L., Canato, S., Jesus, T. T., Goncalves, M., Guerreiro, P. S., Lopes, C. S.,**
998 **Meireles, I., Morais-de-Sa, E., Paredes, J. and Janody, F.** (2023). Activation of an
999 actin signaling pathway in pre-malignant mammary epithelial cells by P-cadherin is
1000 essential for transformation. *Dis Model Mech* **16**.
1001 **Fedor-Chaiken, M., Hein, P. W., Stewart, J. C., Brackenbury, R. and Kinch, M. S.**
1002 (2003). E-cadherin binding modulates EGF receptor activation. *Cell Commun Adhes*
1003 **10**, 105-118.
1004 **Gayrard, C., Bernaudin, C., Dejardin, T., Seiler, C. and Borghi, N.** (2018). Src- and
1005 confinement-dependent FAK activation causes E-cadherin relaxation and beta-catenin
1006 activity. *J Cell Biol* **217**, 1063-1077.
1007 **Gjorevski, N., Piotrowski, A. S., Varner, V. D. and Nelson, C. M.** (2015). Dynamic tensile
1008 forces drive collective cell migration through three-dimensional extracellular
1009 matrices. *Sci Rep* **5**, 11458.
1010 **Gomez, E. W., Chen, Q. K., Gjorevski, N. and Nelson, C. M.** (2010). Tissue geometry
1011 patterns epithelial-mesenchymal transition via intercellular mechanotransduction. *J*
1012 *Cell Biochem* **110**, 44-51.
1013 **Grashoff, C., Hoffman, B. D., Brenner, M. D., Zhou, R., Parsons, M., Yang, M. T.,**
1014 **McLean, M. A., Sligar, S. G., Chen, C. S., Ha, T., et al.** (2010). Measuring
1015 mechanical tension across vinculin reveals regulation of focal adhesion dynamics.
1016 *Nature* **466**, 263-266.
1017 **Han, M. K. L. and de Rooij, J.** (2016). Converging and Unique Mechanisms of
1018 Mechanotransduction at Adhesion Sites. *Trends Cell Biol* **26**, 612-623.
1019 **Hay, B. A., Wolff, T. and Rubin, G. M.** (1994). Expression of baculovirus P35 prevents cell
1020 death in Drosophila. *Development* **120**, 2121-2129.
1021 **He, P., Shen, N., Gao, G., Jiang, X., Sun, H., Zhou, D., Xu, N., Nong, L. and Ren, K.**
1022 (2016). Periodic Mechanical Stress Activates PKCdelta-Dependent EGFR Mitogenic
1023 Signals in Rat Chondrocytes via PI3K-Akt and ERK1/2. *Cell Physiol Biochem* **39**,
1024 1281-1294.
1025 **Hirata, H., Gupta, M., Vedula, S. R., Lim, C. T., Ladoux, B. and Sokabe, M.** (2015).
1026 Actomyosin bundles serve as a tension sensor and a platform for ERK activation.
1027 *EMBO Rep* **16**, 250-257.
1028 **Hirsch, H. A., Iliopoulos, D., Tsichlis, P. N. and Struhl, K.** (2009). Metformin selectively
1029 targets cancer stem cells, and acts together with chemotherapy to block tumor growth
1030 and prolong remission. *Cancer Res* **69**, 7507-7511.
1031 **Horton, E. R., Humphries, J. D., James, J., Jones, M. C., Askari, J. A. and Humphries,**
1032 **M. J.** (2016). The integrin adhesome network at a glance. *J Cell Sci* **129**, 4159-4163.
1033 **Humphries, J. D., Wang, P., Streuli, C., Geiger, B., Humphries, M. J. and Ballestrem,**
1034 **C.** (2007). Vinculin controls focal adhesion formation by direct interactions with talin
1035 and actin. *J Cell Biol* **179**, 1043-1057.
1036 **Jasaitis, A., Estevez, M., Heysch, J., Ladoux, B. and Dufour, S.** (2012). E-cadherin-
1037 dependent stimulation of traction force at focal adhesions via the Src and PI3K
1038 signaling pathways. *Biophys J* **103**, 175-184.
1039 **Kartenbeck, J., Schmid, E., Franke, W. W. and Geiger, B.** (1982). Different modes of
1040 internalization of proteins associated with adhaerens junctions and desmosomes:

1041 experimental separation of lateral contacts induces endocytosis of desmosomal plaque
1042 material. *EMBO J* **1**, 725-732.
1043 **Kruse, K. and Komarova, Y. A.** (2015). Tension across adherens junctions: when less is
1044 more. *Oncotarget* **6**, 30433-30434.
1045 **Kudo, S., Caaveiro, J. M., Nagatoishi, S., Miyafusa, T., Matsuura, T., Sudou, Y. and**
1046 **Tsumoto, K.** (2017). Disruption of cell adhesion by an antibody targeting the cell-
1047 adhesive intermediate (X-dimer) of human P-cadherin. *Sci Rep* **7**, 39518.
1048 **Kumper, S. and Ridley, A. J.** (2010). p120ctn and P-cadherin but not E-cadherin regulate
1049 cell motility and invasion of DU145 prostate cancer cells. *PLoS One* **5**, e11801.
1050 **Kuwahara, K., Kinoshita, H., Kuwabara, Y., Nakagawa, Y., Usami, S., Minami, T.,**
1051 **Yamada, Y., Fujiwara, M. and Nakao, K.** (2010). Myocardin-related transcription
1052 factor A is a common mediator of mechanical stress- and neurohumoral stimulation-
1053 induced cardiac hypertrophic signaling leading to activation of brain natriuretic
1054 peptide gene expression. *Mol Cell Biol* **30**, 4134-4148.
1055 **Lysne, D., Johns, J., Walker, A., Ecker, R., Fowler, C. and Lawson, K. R.** (2014). P-
1056 cadherin potentiates ligand-dependent EGFR and IGF-1R signaling in dysplastic and
1057 malignant oral keratinocytes. *Oncol Rep* **32**, 2541-2548.
1058 **Martinez-Rico, C., Pincet, F., Thiery, J. P. and Dufour, S.** (2010). Integrins stimulate E-
1059 cadherin-mediated intercellular adhesion by regulating Src-kinase activation and
1060 actomyosin contractility. *J Cell Sci* **123**, 712-722.
1061 **Maruthamuthu, V., Sabass, B., Schwarz, U. S. and Gardel, M. L.** (2011). Cell-ECM
1062 traction force modulates endogenous tension at cell-cell contacts. *Proc Natl Acad Sci*
1063 *U S A* **108**, 4708-4713.
1064 **Mendonsa, A. M., Na, T. Y. and Gumbiner, B. M.** (2018). E-cadherin in contact inhibition
1065 and cancer. *Oncogene* **37**, 4769-4780.
1066 **Mertz, A. F., Che, Y., Banerjee, S., Goldstein, J. M., Rosowski, K. A., Revilla, S. F.,**
1067 **Niessen, C. M., Marchetti, M. C., Dufresne, E. R. and Horsley, V.** (2013).
1068 Cadherin-based intercellular adhesions organize epithelial cell-matrix traction forces.
1069 *Proc Natl Acad Sci U S A* **110**, 842-847.
1070 **Mohan, A., Schlue, K. T., Kniffin, A. F., Mayer, C. R., Duke, A. A., Narayanan, V.,**
1071 **Arsenovic, P. T., Bathula, K., Danielsson, B. E., Dumbali, S. P., et al.** (2018).
1072 Spatial Proliferation of Epithelial Cells Is Regulated by E-Cadherin Force. *Biophys J*
1073 **115**, 853-864.
1074 **Montemurro, M., Monier, B. and Suzanne, M.** (2025). The mechanical state of pre-
1075 tumoral epithelia controls subsequent Drosophila tumor aggressiveness. *Dev Cell* **60**,
1076 1036-1052 e1037.
1077 **Moro, L., Venturino, M., Bozzo, C., Silengo, L., Altruda, F., Beguinot, L., Tarone, G.**
1078 **and Defilippi, P.** (1998). Integrins induce activation of EGF receptor: role in MAP
1079 kinase induction and adhesion-dependent cell survival. *EMBO J* **17**, 6622-6632.
1080 **Muhamed, I., Wu, J., Sehgal, P., Kong, X., Tajik, A., Wang, N. and Leckband, D. E.**
1081 (2016). E-cadherin-mediated force transduction signals regulate global cell
1082 mechanics. *J Cell Sci* **129**, 1843-1854.
1083 **Mui, K. L., Chen, C. S. and Assoian, R. K.** (2016). The mechanical regulation of integrin-
1084 cadherin crosstalk organizes cells, signaling and forces. *J Cell Sci* **129**, 1093-1100.
1085 **Nagafuchi, A. and Tsukita, S.** (1994). The Loss of the Expression of alpha Catenin, the 102
1086 kD Cadherin Associated Protein, in Central Nervous Tissues during Development:
1087 (alpha catenin/cadherin/cell adhesion/CNS). *Dev Growth Differ* **36**, 59-71.
1088 **Narayanan, V., Schappell, L. E., Mayer, C. R., Duke, A. A., Armiger, T. J., Arsenovic,**
1089 **P. T., Mohan, A., Dahl, K. N., Gleghorn, J. P. and Conway, D. E.** (2020). Osmotic

1090 Gradients in Epithelial Acini Increase Mechanical Tension across E-cadherin, Drive
1091 Morphogenesis, and Maintain Homeostasis. *Curr Biol* **30**, 624-633 e624.
1092 **Nicolai, M., Lasbleiz, C. and Dura, J. M.** (2003). Gain-of-function screen identifies a role
1093 of the Src64 oncogene in Drosophila mushroom body development. *J Neurobiol* **57**,
1094 291-302.
1095 **Nose, A. and Takeichi, M.** (1986). A novel cadherin cell adhesion molecule: its expression
1096 patterns associated with implantation and organogenesis of mouse embryos. *J Cell*
1097 *Biol* **103**, 2649-2658.
1098 **Oda, H. and Takeichi, M.** (2011). Evolution: structural and functional diversity of cadherin
1099 at the adherens junction. *J Cell Biol* **193**, 1137-1146.
1100 **Padilla-Parra, S. and Tramier, M.** (2012). FRET microscopy in the living cell: different
1101 approaches, strengths and weaknesses. *Bioessays* **34**, 369-376.
1102 **Pece, S. and Gutkind, J. S.** (2000). Signaling from E-cadherins to the MAPK pathway by
1103 the recruitment and activation of epidermal growth factor receptors upon cell-cell
1104 contact formation. *J Biol Chem* **275**, 41227-41233.
1105 **Posern, G., Sotiropoulos, A. and Treisman, R.** (2002). Mutant actins demonstrate a role for
1106 unpolymerized actin in control of transcription by serum response factor. *Mol Biol*
1107 *Cell* **13**, 4167-4178.
1108 **Provenzano, P. P., Inman, D. R., Eliceiri, K. W. and Keely, P. J.** (2009). Matrix density-
1109 induced mechanoregulation of breast cell phenotype, signaling and gene expression
1110 through a FAK-ERK linkage. *Oncogene* **28**, 4326-4343.
1111 **Rao, T. C., Ma, V. P., Blanchard, A., Urner, T. M., Grandhi, S., Salaita, K. and**
1112 **Mattheyses, A. L.** (2020). EGFR activation attenuates the mechanical threshold for
1113 integrin tension and focal adhesion formation. *J Cell Sci* **133**.
1114 **Ribeiro, A. S., Albergaria, A., Sousa, B., Correia, A. L., Bracke, M., Seruca, R., Schmitt,**
1115 **F. C. and Paredes, J.** (2010). Extracellular cleavage and shedding of P-cadherin: a
1116 mechanism underlying the invasive behaviour of breast cancer cells. *Oncogene* **29**,
1117 392-402.
1118 **Ribeiro, A. S., Carvalho, F. A., Figueiredo, J., Carvalho, R., Mestre, T., Monteiro, J.,**
1119 **Guedes, A. F., Fonseca, M., Sanches, J., Seruca, R., et al.** (2016). Atomic force
1120 microscopy and graph analysis to study the P-cadherin/SFK mechanotransduction
1121 signalling in breast cancer cells. *Nanoscale* **8**, 19390-19401.
1122 **Ribeiro, A. S., Sousa, B., Carreto, L., Mendes, N., Nobre, A. R., Ricardo, S., Albergaria,**
1123 **A., Cameselle-Teijeiro, J. F., Gerhard, R., Soderberg, O., et al.** (2013). P-cadherin
1124 functional role is dependent on E-cadherin cellular context: a proof of concept using
1125 the breast cancer model. *J Pathol* **229**, 705-718.
1126 **Rolland, Y., Marighetti, P., Malinverno, C., Confalonieri, S., Luise, C., Ducano, N.,**
1127 **Palamidessi, A., Bisi, S., Kajiho, H., Troglio, F., et al.** (2014). The CDC42-
1128 interacting protein 4 controls epithelial cell cohesion and tumor dissemination. *Dev*
1129 *Cell* **30**, 553-568.
1130 **Santen, R. J. and Mansel, R.** (2005). Benign breast disorders. *N Engl J Med* **353**, 275-285.
1131 **Schindelin, J., Arganda-Carreras, I., Frise, E., Kaynig, V., Longair, M., Pietzsch, T.,**
1132 **Preibisch, S., Rueden, C., Saalfeld, S., Schmid, B., et al.** (2012). Fiji: an open-
1133 source platform for biological-image analysis. *Nat Methods* **9**, 676-682.
1134 **Schneider, C. A., Rasband, W. S. and Eliceiri, K. W.** (2012). NIH Image to ImageJ: 25
1135 years of image analysis. *Nat Methods* **9**, 671-675.
1136 **Sehgal, P., Kong, X., Wu, J., Sunyer, R., Trepat, X. and Leckband, D.** (2018). Epidermal
1137 growth factor receptor and integrins control force-dependent vinculin recruitment to
1138 E-cadherin junctions. *J Cell Sci* **131**.

1139 **Selvaggio, G., Canato, S., Pawar, A., Monteiro, P. T., Guerreiro, P. S., Bras, M. M.,**
1140 **Janody, F. and Chaouiya, C.** (2020). Hybrid Epithelial-Mesenchymal Phenotypes
1141 Are Controlled by Microenvironmental Factors. *Cancer Res* **80**, 2407-2420.
1142 **Shafraz, O., Xie, B., Yamada, S. and Sivasankar, S.** (2020). Mapping transmembrane
1143 binding partners for E-cadherin ectodomains. *Proc Natl Acad Sci U S A* **117**, 31157-
1144 31165.
1145 **Slovakova, J., Sikora, M., Arslan, F. N., Caballero-Mancebo, S., Krens, S. F. G.,**
1146 **Kaufmann, W. A., Merrin, J. and Heisenberg, C. P.** (2022). Tension-dependent
1147 stabilization of E-cadherin limits cell-cell contact expansion in zebrafish germ-layer
1148 progenitor cells. *Proc Natl Acad Sci U S A* **119**.
1149 **Somogyi, K. and Rorth, P.** (2004). Evidence for tension-based regulation of Drosophila
1150 MAL and SRF during invasive cell migration. *Dev Cell* **7**, 85-93.
1151 **Sousa, B., Pereira, J. and Paredes, J.** (2019). The Crosstalk Between Cell Adhesion and
1152 Cancer Metabolism. *Int J Mol Sci* **20**.
1153 **Sullivan, B., Light, T., Vu, V., Kapustka, A., Hristova, K. and Leckband, D.** (2022).
1154 Mechanical disruption of E-cadherin complexes with epidermal growth factor
1155 receptor actuates growth factor-dependent signaling. *Proc Natl Acad Sci U S A* **119**.
1156 **Tadokoro, S., Shattil, S. J., Eto, K., Tai, V., Liddington, R. C., de Pereda, J. M.,**
1157 **Ginsberg, M. H. and Calderwood, D. A.** (2003). Talin binding to integrin beta tails:
1158 a final common step in integrin activation. *Science* **302**, 103-106.
1159 **Taniuchi, K., Nakagawa, H., Hosokawa, M., Nakamura, T., Eguchi, H., Ohigashi, H.,**
1160 **Ishikawa, O., Katagiri, T. and Nakamura, Y.** (2005). Overexpressed P-
1161 cadherin/CDH3 promotes motility of pancreatic cancer cells by interacting with
1162 p120ctn and activating rho-family GTPases. *Cancer Res* **65**, 3092-3099.
1163 **Tavares, S., Vieira, A. F., Taubenberger, A. V., Araujo, M., Martins, N. P., Bras-**
1164 **Pereira, C., Polonia, A., Herbig, M., Barreto, C., Otto, O., et al.** (2017). Actin
1165 stress fiber organization promotes cell stiffening and proliferation of pre-invasive
1166 breast cancer cells. *Nat Commun* **8**, 15237.
1167 **Van Marck, V., Stove, C., Van Den Bossche, K., Stove, V., Paredes, J., Vander Haeghen,**
1168 **Y. and Bracke, M.** (2005). P-cadherin promotes cell-cell adhesion and counteracts
1169 invasion in human melanoma. *Cancer Res* **65**, 8774-8783.
1170 **Vu, V., Light, T., Sullivan, B., Greiner, D., Hristova, K. and Leckband, D.** (2021). P120
1171 catenin potentiates constitutive E-cadherin dimerization at the plasma membrane and
1172 regulates trans binding. *Curr Biol* **31**, 3017-3027 e3017.
1173 **Wallrabe, H. and Periasamy, A.** (2005). Imaging protein molecules using FRET and FLIM
1174 microscopy. *Curr Opin Biotechnol* **16**, 19-27.
1175 **Wang, H. B., Dembo, M., Hanks, S. K. and Wang, Y.** (2001). Focal adhesion kinase is
1176 involved in mechanosensing during fibroblast migration. *Proc Natl Acad Sci U S A*
1177 **98**, 11295-11300.
1178 **Wei, S. Y., Escudero, L. M., Yu, F., Chang, L. H., Chen, L. Y., Ho, Y. H., Lin, C. M.,**
1179 **Chou, C. S., Chia, W., Modolell, J., et al.** (2005). Echinoid is a component of
1180 adherens junctions that cooperates with DE-Cadherin to mediate cell adhesion. *Dev*
1181 *Cell* **8**, 493-504.
1182 **Yano, S., Komine, M., Fujimoto, M., Okochi, H. and Tamaki, K.** (2004). Mechanical
1183 stretching in vitro regulates signal transduction pathways and cellular proliferation in
1184 human epidermal keratinocytes. *J Invest Dermatol* **122**, 783-790.
1185 **Yao, M., Qiu, W., Liu, R., Efremov, A. K., Cong, P., Seddiki, R., Payre, M., Lim, C. T.,**
1186 **Ladoux, B., Mege, R. M., et al.** (2014). Force-dependent conformational switch of
1187 alpha-catenin controls vinculin binding. *Nat Commun* **5**, 4525.

1188 **Ziegler, W. H., Gingras, A. R., Critchley, D. R. and Emsley, J.** (2008). Integrin
1189 connections to the cytoskeleton through talin and vinculin. *Biochem Soc Trans* **36**,
1190 235-239.
1191 **Zuidema, A., Wang, W. and Sonnenberg, A.** (2020). Crosstalk between Cell Adhesion
1192 Complexes in Regulation of Mechanotransduction. *Bioessays* **42**, e2000119.
1193